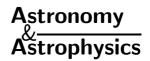
© ESO 2001



# A comparison between theoretical and solar Fe xII UV line intensity ratios\*

A. M. Binello<sup>1</sup>, E. Landi<sup>2</sup>, H. E. Mason<sup>1</sup>, P. J. Storey<sup>3</sup>, and J. W. Brosius<sup>4</sup>

- Department of Applied Mathematics and Theoretical Physics, University of Cambridge, UK
- <sup>2</sup> Naval Research Laboratory, Washington DC, 20375, USA
- <sup>3</sup> Department of Physics and Astronomy, University College London, Gower Street, London WC1E 6BT, UK
- <sup>4</sup> Raytheon ITSS, Laboratory for Astronomy and Solar Physics, Code 682.1, NASA's Goddard Space Flight Center, Greenbelt, MD 20771, USA

Received 18 December 2000 / Accepted 13 February 2001

**Abstract.** A new set of radiative and electron collisional data for Fe XII was presented in two earlier papers. In the present work, we derive level populations and theoretical line intensities for a range of plasma densities and temperatures. Observations of Fe XII lines obtained with the *Solar EUV Rocket Telescope and Spectrograph* are analysed both as a check the quality of the new atomic data and to determine the electron density in active regions and the quiet Sun. The discrepancy between the electron density values determined from Fe XII line intensity ratios and those obtained from other ions is investigated.

**Key words.** Sun: general – atomic data – UV Sun: radiations – plasmas

# 1. Introduction

Spectroscopic diagnostics using UV, EUV and X-ray line intensities are a fundamental tool for the measurement of physical parameters of solar and stellar atmospheres, such as electron density, temperature, plasma differential emission measure and chemical composition. See Mason & Monsignori Fossi (1994) for a comprehensive review. These diagnostics require a large amount of accurate atomic data, including radiative and collisional transition probabilities.

Fe XII plays a key role in diagnostic studies because of its wealth of strong spectroscopic lines covering a wide wavelength range in the UV, EUV and X-ray spectral regions. Flower (1977) (hereafter referred to as F77) was the first to carry out a complete ab initio atomic structure and electron scattering calculation for Fe XII and to compute relative spectral line intensities. He provided collision strengths for all electric dipole and optically forbidden transitions both within the ground  $3s^2 3p^3$  configuration and between this and the first two excited  $3s 3p^4$ ,  $3s^2 3p^2 3d$  configurations. He stressed the usefulness of forbidden line ratios within the ground configuration of Fe XII

Send offprint requests to: E. Landi, e-mail: landi@poppeo.nrl.navy.mil

cdarc.u-strasbg.fr (130.79.128.5) or via

http://cdsweb.u-strasbg.fr/cgi-bin/qcat?J/A+A/370/1071 Harrison et al. 1997; Mason et al. 1997).

for determining the coronal electron density. Improved radiative (Tayal & Henry 1986) and electron collisional data for  $3\mathrm{s}^2 3\mathrm{p}^3$  (Tayal et al. 1987) and  $3\mathrm{s}^2 3\mathrm{p}^3 - 3\mathrm{s} 3\mathrm{p}^4$  (Tayal & Henry 1988) transitions were obtained by using an extended target representation and a more sophisticated collisional approach. These studies pointed to the importance of resonance contributions to the collision strengths and provided a new set of Fe XII level populations.

The use of these Fe XII atomic data has enabled the determination of electron density, temperature and iron abundance in the solar coronal plasma through the analysis of spectra from experiments such as early solar eclipse observations (Gabriel & Jordan 1975), the Goddard OSO-7 spectroheliograph (Kastner & Mason 1978), the Harvard and NRL experiments on board Skylab (Mariska et al. 1980; Feldman et al. 1983; Withbroe & Raymond 1984; Tayal et al. 1989, 1991; Keenan et al. 1990, 1991) and, more recently, the Solar EUV Rocket Telescope and Spectrograph SERTS (Keenan et al. 1996; Young et al. 1998).

It was clear from an assessment of theoretical electron excitation data for various iron ions (Mason 1994) that the Tayal & Henry (1986) and Tayal et al. (1987) electron scattering calculations suffered from some anomalies and limitations. Our new set of Fe XII atomic computations were carried out as part of the *IRON Project* (Hummer et al. 1993) in response to the need for improved atomic data required to analyse the SOHO spectra (Mason 1994; Harrison et al. 1997; Mason et al. 1997).

 $<sup>^{\</sup>star}$  Tables 2–5 are also available in electronic form at the CDS via anonymous ftp to

Atomic structure and electron scattering results have been presented in two previous papers (Binello et al. 1998a, 1998b, henceforth referred to as BMSI and BMSII respectively), together with a thorough discussion of the computational methods. In the present work we have complemented this dataset with new atomic data, in order to to improve the Fe XII atomic model further. We have derived accurate theoretical line intensity ratios for comparison with the observed values obtained from high resolution solar spectra. One aim of this study is to check the quality of our new atomic data, in order to reveal line blends in the spectra through density insensitive line ratios and to derive the electron density in the solar atmosphere by using density sensitive line ratios.

Another aim of the present work is to investigate the causes of the discrepancy that has been noted between density values derived using Fe XII lines and those determined using spectral lines from other ions (Landi & Landini 1997, 1998; Brosius et al. 1998a, 1998b). Fe XII density values appear to be higher than those provided by Fe XI, Fe XIII, Fe XIV and Si X by a factor between 3 and 10, according to the emitting solar feature.

We have compared our theoretical line emissivities with observations of Fe XII lines obtained with the SERTS instrument in 1989 (Thomas & Neupert 1994) and 1995 (Brosius et al. 1998b). Line emissivities calculated using Flower (1977) (F77), Tayal et al. (1987), Tayal & Henry (1988), and an improved Fe XII model developed in the present work, are also used in order to check differences in the resulting electron densities. Fe XII density values are compared with those obtained with other ions.

The present paper is structured as follows. Section 2 reviews the calculations of Fe XII atomic data already existing in the literature. Section 3 introduces the atomic data used in the present work. A comparison between these atomic data and those available in the literature is given in Sect. 4. Section 5 describes the SERTS observations. The theoretical intensity ratios are discussed in Sect. 6. Sections 7 to 8 present the comparison between theoretical and observed line intensity ratios. The Fe XII line ratios yield higher electron density values than those from other ions. Section 9 describes an improvement to the atomic model proposed to address this discrepancy, and compares the results with the observations. Results are summarized in Sect. 10.

#### 2. Fe XII calculations in the literature

The first theoretical collision strengths for electron excitation of the Fe<sup>+11</sup> ion were the result of numerical work by Czyzak & Krueger (1967) and Blaha (1969), for transitions between LS coupling terms and fine structure levels, respectively. Later, new collision strengths were computed by Czyzak et al. (1970) and Krueger & Czyzak (1970), between LS coupling target terms as well as intermediate coupling target levels, using the distorted wave method. Forbidden transitions within the ground  $3s^2 3p^3$  configuration were considered in those calculations. Improved

collision strengths for selected 3s<sup>2</sup>3p<sup>3</sup>–3s3p<sup>4</sup> optically allowed transitions between target terms and fine structure levels were given by Davis et al. (1976), again within the distorted wave approach.

A major breakthrough in the computation of intermediate coupling electron excitation data for Fe XII was represented by the work of F77, also within the distorted wave approximation, and of Tayal et al. (1987) and Tayal & Henry (1988), using the close-coupling approximation. F77 used a very simple target model, including the two odd parity  $3s^2 3p^3$ ,  $3p^5$  and the two even parity  $3s 3p^4$ ,  $3s^2 3p^2 3d$  configurations, and computed collision strengths at only one energy of the colliding electron (6.6 Ry). Collisional data were published for the optically forbidden  $3s^2 3p^3$  transitions and for all possible forbidden and electric dipole transitions between the configurations:  $3s^2 3p^3 - 3s 3p^4$  and  $3s^2 3p^3 - 3s^2 3p^2 3d$ . For the former, allowance was made for resonance effects in the cross sections by using the approximate method of Petrini (1970).

The more sophisticated R-matrix technique was used by Tayal et al. (1987) to compute collision strengths and effective collision strengths, obtained by integrating the former over a Maxwellian distribution of electron energies, for the forbidden 3s<sup>2</sup> 3p<sup>3</sup> fine structure transitions. A more comprehensive target, described by Tayal & Henry (1986), included all possible configurations with up to two  $\overline{3}d$  electrons, as well as the  $3s^2 3p^2 \overline{4}f$  and  $3s 3p^3 \overline{4}f$  configurations. The lowest seven LS coupling target states, those belonging to the 3s<sup>2</sup>3p<sup>3</sup>, 3s3p<sup>4</sup> configurations, were included in the expansion of the total wavefunction. Maxwellianaveraged collision strengths were given for the electron temperature range 4  $10^5$ –3  $10^6$  K. The importance of a proper, ab initio treatment of the resonance problem in the scattering computation was stressed in their paper. Subsequently Tayal & Henry (1988) published analogous results for all possible  $3s^2 3p^3 - 3s 3p^4$  transitions.

The R-matrix scattering data from Tayal et al. (1987) and Tayal & Henry (1988) have been the most popular and widely used in astrophysical and laboratory applications. However, Mason (1994), in her assessment of theoretical electron excitation data for various iron ions, pointed out some unusual features in those results, which have never been explained. This, along with the fact that new scattering data for the  $3s^2 3p^3 - 3s^2 3p^2 3d$  transitions had not been computed since the rather approximate results of F77, triggered the new set of R-matrix calculations carried out by BMSI and BMSII and described in the next section.

# 3. Atomic data

# 3.1. Energies and spontaneous decay rates

The Fe XII model used in the present work consists of 41 fine structure levels, those belonging to the  $3s^2 3p^3$ ,  $3s 3p^4$ ,  $3s^2 3p^2 3d$  configurations. Theoretical excitation energies, oscillator strengths and spontaneous transition

**Table 1.** Energy levels  $(cm^{-1})$  for the lowest three configurations in Fe XII. For values in *italic* see text

Configuration	Level	$E_{ m th}$	$E_{\rm obs}$
O		(set 3A)	000
$3s^2 3p^3$	${}^{4}S^{o}_{3/2}$	0	0
•	$^{2}D_{3/2}^{0}$	42789	41555
	${}^{2}\mathrm{D}_{5/2}^{0/2}$	46907	46088
	${}^{2}\mathrm{P}_{1/2}^{0/2}$	76895	74108
	${}^{2}\mathrm{P}_{3/2}^{0/2}$	82587	80515
$3s 3p^4$	${}^{4}P_{5/2}$	274389	274373
<b>T</b>	${}^{4}\mathrm{P}_{3/2}$	283883	284005
	${}^{4}\mathrm{P}_{1/2}$	288235	288307
	${}^{2}\mathrm{D}_{3/2}^{1/2}$	341900	339761
	${}^{2}\mathrm{D}_{5/2}$	343595	341703
	${}^{2}\mathrm{P}_{3/2}^{3/2}$	394281	389668
	${}^{2}\mathrm{P}_{1/2}$	399595	394352
	${}^{2}S_{1/2}$	415694	410401
$3s^2 3p^2 3d$	$(^{9}P) ^{4}F_{3/2}$	431849	419577
*	$(^{3}P)  ^{4}F_{5/2}$	435616	423344
	$(^{3}P)  ^{4}F_{7/2}$	441131	428859
	$(^{1}D)  ^{2}F_{5/2}$	449292	435616
	$(^{3}P)^{4}F_{0/2}$	447979	435707
	$(^{3}P)^{4}D_{1/2}$	452638	440366
	$(^{3}P)^{4}D_{7/2}$	453159	440887
	$(^{3}P)^{4}D_{3/2}$	453713	441441
	$(^{3}P)^{4}D_{5/2}$	458342	446070
	$(^{1}D)  ^{2}F_{7/2}$	468104	454428
	$(^{1}D)  ^{2}G_{7/2}$	503510	489834
	$(^{1}D)^{2}G_{9/2}$	506378	492702
	$(^{3}P)^{2}P_{3/2}$	511268	501800
	$(^{3}P)^{4}P_{5/2}^{3/2}$	521908	512510
	$(^{3}P)^{2}P_{1/2}$	523255	513850
	$(^{3}P)  ^{4}P_{3/2}$	526123	516740
	$(^{3}P)^{4}P_{1/2}$	528826	519770
	$(^{1}S) ^{2}D_{3/2}$	537312	526120
	$(^{1}S)  ^{2}D_{5/2}$	547826	538040
	$(^{1}D)^{2}D_{3/2}$	565364	554030
	$(^{1}D)^{2}D_{5/2}$	566648	554610
	$(^{1}D)^{2}P_{1/2}$	586413	568940
	$(^{3}P)^{2}F_{5/2}$	590771	576740
	$(^{1}D)^{2}P_{3/2}$	594486	577740
	$(^{1}D)^{2}S_{1/2}$	592965	579630
	$(^{3}P)^{2}F_{7/2}$	595133	581180
	$(^{3}P)^{2}D_{5/2}$	618968	603930
	$(^{3}P)^{2}D_{3/2}^{3/2}$	620649	605480

**Table 2.** Spontaneous transition probabilities for all electric dipole fine structure transitions between the ground  $3s^2 3p^3$  and the first excited  $3s 3p^4$  configurations in Fe XII. Numbers in parenthesis are powers of 10. Wavelengths are taken from CHIANTI (Dere et al. 1997; Landi et al. 1999)

	,	,
Transition	Wavelengths	A
$(3s 3p^4 \rightarrow 3s^2 3p^3)$	(Å)	$(s^{-1})$
${}^{4}\mathrm{P}_{5/2} - {}^{4}\mathrm{S}^{\mathrm{o}}_{3/2}$	364.47	1.589 (9)
${}^{4}\mathrm{P}_{3/2} - {}^{4}\mathrm{S}_{3/2}^{\mathrm{o}}$	352.11	1.728(9)
${}^{4}P_{1/2} - {}^{4}S_{3/2}^{o}$	346.85	1.814(9)
$^{2}D_{3/2} - ^{4}S_{3/2}^{o}$	294.33	3.834(6)
${}^{2}\mathrm{D}_{5/2} - {}^{4}\mathrm{S}_{3/2}^{0/2}$	292.65	7.599(6)
$^{2}P_{3/2} - ^{4}S_{3/2}^{o}$	256.63	4.124(7)
$^{2}P_{1/2} - ^{4}S_{3/2}^{o}$	253.58	3.877(7)
$^{2}S_{1/2} - ^{4}S_{3/2}^{o}$	243.66	7.977(7)
$P_{5/2} = D_{3/2}$	429.52	1.156(7)
${}^{4}P_{3/2} - {}^{2}D_{3/2}^{o}$	412.46	8.332(5)
$^{4}P_{1/2} - ^{2}D_{3/2}^{o}$	405.27	4.818(6)
$^{2}D_{2/2} - ^{2}D_{2/2}^{0}$	335.34	3.330(9)
$^{2}D_{5/2} - ^{2}D_{2/2}^{o}$	333.17	3.260(7)
$^{2}P_{3/2} - ^{2}D_{3/2}^{\circ}$	287.26	8.917(8)
$^{2}P_{1/2} - ^{2}D_{3/2}^{\circ}$	283.45	7.272(9)
$^{2}S_{1/2} - ^{2}D_{3/2}^{o}$	271.12	2.948(8)
$^{4}P_{5/2} - ^{2}D_{5/2}^{o}$	430.05	2.132(7)
$^{4}P_{3/2} - ^{2}D_{5/2}^{o}$	420.32	3.916(6)
$^{2}D_{3/2} - ^{2}D_{5/2}^{o}$	340.51	4.769(7)
$^{2}D_{5/2} - ^{2}D_{5/2}^{o}$	338.28	2.759(9)
$^{2}P_{3/2} - ^{2}D_{5/2}^{o}$	291.05	7.561(9)
$^{4}P_{3/2} - ^{2}P_{1/2}^{o}$	476.42	1.124(5)
$^{4}P_{1/2} - ^{2}P_{1/2}^{o}$	466.86	8.777(6)
$^{2}D_{3/2} - ^{2}P_{1/2}^{o}$	376.43	2.838(8)
$^{2}P_{3/2} - ^{2}P_{1/2}^{o}$	316.90	3.686(8)
$^{2}P_{1/2} - ^{2}P_{1/2}^{o}$	312.26	3.231(9)
$^{2}S_{1/2} - ^{2}P_{1/2}^{o}$	297.36	1.001(9)
$^{4}P_{5/2} - ^{2}P_{3/2}^{o}$	515.84	2.094(6)
$^{4}P_{3/2} - ^{2}P_{3/2}^{o}$	491.43	9.149(6)
$^{4}P_{1/2} - ^{2}P_{3/2}^{o}$	481.25	1.382(6)
$^{2}D_{3/2} - ^{2}P_{3/2}^{o}$	385.73	1.241(7)
$^{2}D_{5/2} - ^{2}P_{3/2}^{o}$	382.87	5.535(8)
$^{2}P_{3/2} - ^{2}P_{3/2}^{o}$	323.46	6.773(8)
2D 2D0	910.64	1 991 (7)
${}^{2}P_{1/2} - {}^{2}P_{3/2}^{o}$ ${}^{2}S_{1/2} - {}^{2}P_{3/2}^{o}$	318.64 $303.14$	1.231 (7) 7.252 (9)

probabilities have been computed with the atomic structure program SUPERSTRUCTURE (Eissner et al. 1974; Nussbaumer & Storey 1978).

Details of the structure computations and, in particular, of the choice of configurations included in the wavefunction basis expansion can be found in BMSI. The following set of configurations (set 3A in BMSI) were used:

 $3s^{2} 3p^{3}, 3s 3p^{4}, 3s^{2} 3p^{2} 3d, 3p^{5}, \\ 3s 3p^{3} 3d, 3p^{4} 3d, 3s 3p^{2} 3d^{2}, 3p^{3} 3d^{2}, \\ 3s^{2} 3p 3d^{2}, 3s^{2} 3d^{3}, 3s 3p 3d^{3}, 3p^{2} 3d^{3}, \\ 3s^{2} 3p^{2} \overline{4}l, 3s 3p^{3} \overline{4}l, 3p^{4} \overline{4}l,$ 

where  $\overline{4l}$  represents  $\overline{4s}$ ,  $\overline{4p}$ ,  $\overline{4d}$  and  $\overline{4f}$  correlation orbitals (hydrogenic).

In Table 1 we list all the fine structure levels included in the present model along with the relative experimental energy values, taken from Corliss & Sugar (1982) and Jupén et al. (1993), and the theoretical energy values obtained with set 3A. Italic type in the column listing  $E_{\rm obs}$  has been adopted to indicate those levels whose experimental energies are not yet known; in these cases the corresponding theoretical energies listed in Table 1 were empirically adjusted with the procedure described in BMSI. There is a slight difference with the  $E_{\rm obs}$  listed in BMSI (Table 3), since the set 3, rather than set 3A was adjusted in that paper. Line strengths were computed with set 3A

**Table 3.** Spontaneous transition probabilities for all electric dipole fine structure transitions between the ground  $3s^2 3p^3$  and the second excited  $3s^2 3p^2 3d$  configurations in Fe XII. the numbers in parenthesis in the column of A values are powers of 10. For a see text. Wavelengths are taken from the CHIANTI database (Dere et al. 1997; Landi et al. 1999). Wavelengths in italics are calculated from theoretical energy levels, as no experimental energy is available

Transition	Wavelength	A	Transition	Wavelength	A
$(3s^2 3p^2 3d \rightarrow 3s^2 3p^3)$	(Å)	$(s^{-1})$	$(3s^2 3p^2 3d \rightarrow 3s^2 3p^3)$	(Å)	$(s^{-1})$
$(^{3}P)  ^{4}F_{3/2} - ^{4}S_{3/2}^{o}$	237.95	1.399(7)	$(^{1}\mathrm{D})^{2}\mathrm{F}_{7/2}$ – $^{2}\mathrm{D}_{5/2}^{\mathrm{o}}{}^{a}$	244.02	7.315(3)
$(^{3}P)^{4}F_{5/2} - ^{4}S_{3/2}^{o}$	235.84	2.717(7)	$(^{1}D)^{2}G_{7/2} - ^{2}D_{5/2}^{o}$	224.31	2.212 (8)
$(^{1}D)^{2}F_{5/2} - {}^{4}S_{3/2}^{o}$	228.73	1.016 (8)	$(^{3}P)^{2}P_{3/2} - ^{2}D_{5/2}^{0/2}$	219.44	4.540 (10)
$(^{3}P)^{4}D_{1/2} - ^{4}S_{3/2}^{o}$	227.11	6.299(7)	$(^{3}P)^{4}P_{5/2} - ^{2}D_{5/2}^{o}$	214.40	1.292(9)
$(^{3}P)^{4}D_{3/2} - ^{4}S_{3/2}^{o}$	226.55	2.581 (8)	$(^{3}P)^{4}P_{3/2} - ^{2}D_{5/2}^{o/2}$	212.47	2.829 (8)
$(^{3}P)  ^{4}D_{5/2} - ^{4}S_{3/2}^{o}$	224.19	2.767(8)	$(^{1}S)^{2}D_{3/2} - ^{2}D_{5/2}^{o}$	208.32	6.089(9)
$(^{3}P)^{2}P_{3/2}^{3/2} - ^{4}S_{3/2}^{0/2}$	199.28	2.406 (8)	$(^{1}S)^{2}D_{5/2}^{5/2} - ^{2}D_{5/2}^{0}$	203.27	3.080 (10)
$(^{3}P)  ^{4}P_{5/2} - ^{4}S_{3/2}^{o}$	195.12	8.638 (10)	$(^{1}D)^{2}D_{3/2}^{3/2} - ^{2}D_{5/2}^{o}$	196.87	9.306(9)
$(^{3}P)^{2}P_{1/2} - ^{4}S_{3/2}^{o}$	194.61	5.086 (9)	$(^{1}D)^{2}D_{5/2}^{7} - {^{2}D_{5/2}^{0}}$	196.65	4.070 (10)
$(^{3}P)  ^{4}P_{3/2} - ^{4}S_{3/2}^{o}$	193.52	8.901 (10)	$(^{3}P)^{2}F_{5/2} - ^{2}D_{5/2}^{o}$	188.45	5.721 (9)
$(^{3}P)^{4}P_{1/2} - ^{4}S_{3/2}^{o}$	192.39	8.807 (10)	$(^{1}D)^{2}P_{3/2} - ^{2}D_{5/2}^{o}$	188.09	5.617(8)
$(^{1}S)^{2}D_{3/2} - {^{4}S_{3/2}^{o}}$	190.07	2.955(9)	$(^{3}P)^{2}F_{7/2} - ^{2}D_{5/2}^{o}$	186.88	1.067 (11)
$(^{1}S)^{2}D_{5/2} - ^{4}S_{3/2}^{o}$	185.86	2.563(9)	$(^{3}P)^{2}D_{5/2} - ^{2}D_{5/2}^{\circ}$	179.26	4.552(9)
$(^{1}D)^{2}D_{3/2} - {}^{4}S_{3/2}^{o}$	180.50	2.536(5)	$(^{3}P)^{2}D_{3/2} - ^{2}D_{5/2}^{o/2}$	178.77	2.169(8)
$(^{1}D)^{2}D_{5/2} - {}^{4}S_{3/2}^{o}$	180.31	6.934(7)	$(^{3}P)^{4}F_{3/2} - ^{2}P_{1/2}^{o}$	288.89	1.585(7)
$(^{1}D)^{2}P_{1/2} - {}^{4}S_{3/2}^{o'}$	175.77	4.606(7)	$(^{3}P)^{4}D_{1/2} - ^{2}P_{1/2}^{o}$	273.07	3.259(7)
$(^{3}P)^{2}F_{5/2} - ^{4}S_{3/2}^{o'}$	193.39	3.300(8)	$(^{3}P)^{4}D_{3/2} - ^{2}P_{1/2}^{o'}$	272.35	6.624(6)
$(^{1}D)^{2}P_{3/2} - {^{4}S_{3/2}}^{\circ}$	173.09	5.912(7)	$(^{3}P)^{2}P_{3/2} - ^{2}P_{1/2}^{o}$	233.81	1.419 (9)
$(^{1}D) {^{2}S_{1/2}} - {^{4}S_{3/2}}$	172.52	1.074(5)	$(^{3}P)^{2}P_{1/2} - ^{2}P_{1/2}^{0}$	227.41	8.293 (9)
$(^{3}P)^{2}D_{5/2} - ^{4}S_{3/2}^{o}$	165.58	3.866(8)	$(^{3}P) {^{4}P_{3/2}} - {^{2}P_{1/2}^{0}}$	225.92	6.352(6)
$(^{3}P)^{2}D_{3/2} - ^{4}S_{3/2}^{o}$	165.12	7.179(7)	$(^{3}P)  ^{4}P_{1/2} - ^{2}P_{1/2}^{o}$	224.39	4.868 (8)
$(^{3}P)^{4}F_{3/2} - ^{2}D_{3/2}^{o}$	264.06	1.417(8)	$(^{1}S)^{2}D_{3/2} - ^{2}P_{1/2}^{o}$	221.23	1.003(8)
$(^{3}P)  ^{4}F_{5/2} - ^{2}D_{3/2}^{o'}$	261.45	1.641(7)	$(^{1}\mathrm{D})^{2}\mathrm{D}_{3/2}-{}^{2}\mathrm{P}_{1/2}^{\circ}$	208.37	6.636(9)
$(^{1}D)^{2}F_{5/2} - ^{2}D_{3/2}^{o}$	252.76	8.246 (5)	$(^{1}D)^{2}P_{1/2} - ^{2}P_{1/2}^{o}$	202.09	6.422(10)
$(^{3}P)^{4}D_{1/2}^{-2} - ^{2}D_{3/2}^{0}$	250.78	3.738 (8)	$(^{1}D)^{2}P_{3/2} - {^{2}P_{1/2}^{o}}$	198.56	1.850 (10)
$(^{3}P)^{4}D_{3/2} - ^{2}D_{3/2}^{o}$	250.09	6.449(5)	$(^{1}D)^{2}S_{1/2} - ^{2}P_{1/2}^{o}$	197.82	5.149 (8)
$(^{3}P)  ^{4}D_{5/2} - ^{2}D_{3/2}^{o}$	247.22	2.377(6)	$(^{3}P)^{2}D_{2/2} - ^{2}P_{1/2}^{o}$	188.19	7.028 (10)
$(^{3}P)^{2}P_{3/2} - ^{2}D_{3/2}^{o}$	217.28	1.855 (10)	$(^{3}P)^{4}F_{3/2} - ^{2}P_{3/2}^{o}$	294.34	1.055 (6)
$(^{3}P)^{4}P_{5/2} - ^{2}D_{3/2}^{o}$	212.34	3.433(8)	$(^{3}P)^{4}F_{5/2} - ^{2}P_{3/2}^{0}$	291.12	9.382(6)
$(^{3}P)^{2}P_{1/2} - ^{2}D_{3/2}^{o'}$	211.73	4.323(10)	$(^{1}D) {^{2}F_{5/2}} - {^{2}P_{3/2}^{o}}$	280.36	5.128(6)
$(^{3}P)  ^{4}P_{3/2} - ^{2}D_{3/2}^{o}$	210.44	2.251(8)	$(^{3}P) ^{4}D_{1/2} - ^{2}P_{3/2}^{o}$	277.93	1.379(8)
$(^{3}P)  ^{4}P_{1/2} - ^{2}D_{3/2}^{o}$	209.11	4.060(9)	$(^{3}P)  ^{4}D_{3/2} - ^{2}P_{3/2}^{o}$	277.09	2.499(7)
$(^{1}S)^{2}D_{3/2} - ^{2}D_{3/2}^{o}$	206.37	9.166(9)	$(^{3}P)  ^{4}D_{5/2} - ^{2}P_{3/2}^{o}$	273.57	2.479(6)
$(^{1}S)  ^{2}D_{5/2} - ^{2}D_{3/2}^{o}$	201.42	7.277(8)	$(^{3}P)^{2}P_{3/2} - ^{2}P_{3/2}^{o}$	237.37	4.585(9)
$(^{1}\mathrm{D})^{2}\mathrm{D}_{3/2}-^{2}\mathrm{D}_{3/2}^{\circ}$	195.13	5.712(10)	$(^{3}P)  ^{4}P_{5/2} - ^{2}P_{3/2}^{o}$	231.48	2.026(6)
$(^{1}D)^{2}D_{5/2} - ^{2}D_{3/2}^{o}$	194.91	2.271(9)	$(^{3}P)^{2}P_{1/2} - ^{2}P_{3/2}^{o}$	230.77	1.422(10)
$(^{1}D)^{2}P_{1/2} - ^{2}D_{3/2}^{o}$	189.62	2.064(9)	$(^{3}P)^{4}P_{3/2} - ^{2}P_{3/2}^{o}$	229.24	1.397(8)
$(^{3}P)^{2}F_{5/2} - ^{2}D_{3/2}^{o}$	186.85	1.002(11)	$(^{3}P)  ^{4}P_{1/2} - ^{2}P_{3/2}^{o}$	227.66	5.717(8)
$(^{1}D)^{2}P_{3/2} - ^{2}D_{3/2}^{o}$	186.50	1.423(9)	$(^{1}S) {^{2}D_{3/2}} - {^{2}P_{3/2}^{o}}$	224.41	2.939(8)
$(^{1}D)^{2}S_{1/2} - ^{2}D_{3/2}^{o}$	185.85	8.178(9)	$(^{1}S)^{2}D_{5/2} - ^{2}P_{3/2}^{o}$	218.57	2.978(9)
$(^{3}P)  ^{2}D_{5/2} - ^{2}D_{3/2}^{\circ}$	177.82	7.159(7)	$(^{1}D)^{2}D_{3/2} - ^{2}P_{3/2}^{o}$	211.19	2.913(8)
$(^{3}P)^{2}D_{3/2} - ^{2}D_{3/2}^{o'}$	177.33	2.814(8)	$(^{1}D)^{2}D_{5/2} - ^{2}P_{3/2}^{o}$	210.93	4.270(9)
$(^{3}P)  ^{4}F_{3/2} - ^{2}D_{5/2}^{o'}$	267.26	1.532(6)	$(^{1}D) {^{2}P_{1/2}} - {^{2}P_{3/2}^{o}}$	204.74	5.724(8)
$(^{3}P)  ^{4}F_{5/2} - ^{2}D_{5/2}^{o'}$	264.60	4.171(7)	$(^{3}P)^{2}F_{5/2} - ^{2}P_{3/2}^{o}$	201.52	2.252(8)
$(^{3}P)  ^{4}F_{7/2} - ^{2}D_{5/2}^{o}$	260.80	2.091(7)	$(^{1}D)  ^{2}P_{3/2} - ^{2}P_{3/2}^{o}$	201.12	4.989(10)
$(^{1}\mathrm{D})^{2}\mathrm{F}_{5/2}-^{2}\mathrm{D}_{5/2}^{o}{}^{a}$	255.69	4.992(3)	$(^{1}D) {^{2}S_{1/2}} - {^{2}P_{3/2}^{o}}$	200.36	6.209(10)
$(^{3}P)  ^{4}D_{7/2} - ^{2}D_{5/2}^{o}$	253.26	2.886(7)	$(^{3}P)^{2}D_{5/2} - ^{2}P_{3/2}^{o}$	191.05	9.023(10)
$(^{3}P)  ^{4}D_{3/2} - ^{2}D_{5/2}^{o}$	252.96	3.048(8)	$(^{3}P)^{2}D_{3/2} - ^{2}P_{3/2}^{o'}$	190.49	2.220(10)
$(^{3}P)^{4}D_{5/2} - ^{2}D_{5/2}^{o'}$	250.02	8.309(7)	•		

**Table 4.** Spontaneous transition probabilities for the 10 optically forbidden fine structure transitions within the ground  $3s^2\,3p^3$  configuration of Fe XII. Numbers in parenthesis are powers of 10. The wavelengths are from CHIANTI

Transition	Wavelength	Transition	A
	(Å)	type	$(s^{-1})$
$^{2}\mathrm{D}^{\mathrm{o}}_{3/2}$ – $^{4}\mathrm{S}^{\mathrm{o}}_{3/2}$	2406.45	M1	4.419(1)
$^{2}\mathrm{D}_{5/2}^{\mathrm{o'}}-{}^{4}\mathrm{S}_{3/2}^{\mathrm{o'}}$	2169.76	M1	1.826(0)
${}^{2}\mathrm{P}_{1/2}^{\mathrm{o'}} - {}^{4}\mathrm{S}_{3/2}^{\mathrm{o'}}$	1349.38	M1	1.665(2)
${}^{2}\mathrm{P}_{3/2}^{\mathrm{o}'} - {}^{4}\mathrm{S}_{3/2}^{\mathrm{o}'}$	1242.01	M1	3.214(2)
$^{2}\mathrm{D}_{5/2}^{o'}-{^{2}\mathrm{D}_{3/2}^{o'}}$	22060.45	M1	8.945(-1)
${}^{2}\mathrm{P}_{1/2}^{o'} - {}^{2}\mathrm{D}_{3/2}^{o'}$	3071.91	M1	6.427(1)
${}^{2}\mathrm{P}_{3/2}^{\mathrm{o}'} - {}^{2}\mathrm{D}_{3/2}^{\mathrm{o}'}$	2566.74	M1	1.799(2)
${}^{2}\mathrm{P}_{1/2}^{o'} - {}^{2}\mathrm{D}_{5/2}^{o'}$	3568.88	E2	2.971(-1)
${}^{2}\mathrm{P}_{3/2}^{o} - {}^{2}\mathrm{D}_{5/2}^{o}$	2904.70	M1	7.277(1)
${}^{2}\mathrm{P}_{3/2}^{o'} - {}^{2}\mathrm{P}_{1/2}^{o'}$	15607.93	M1	2.069(0)

and combined with the experimental energies listed in Table 1 to obtain radiative transition probabilities. A list of spontaneous decay rates so obtained is presented in Table 2 for all the electric dipole (E1)  $3s^2 3p^3 - 3s 3p^4$  fine structure transitions and in Table 3 for all the E1  $3s^2 3p^3 - 3s^2 3p^2 3d$  fine structure transitions.

In Table 4 we list the decay rates for the ten  $3s^2 3p^3$  fine structure optically forbidden transitions, corresponding to spectral lines which have been frequently recorded in UV solar spectra. For the optically forbidden transitions either between levels within a configuration or between levels of the two excited 3s 3p<sup>4</sup>, 3s<sup>2</sup> 3p<sup>2</sup> 3d configurations the electric quadrupole (E2) and magnetic dipole (M1) components have been summed to give the total decay rate  $A_{\text{tot}} = A(\text{E2}) + A(\text{M1})$ . The remaining optically forbidden transitions included are magnetic quadrupole (M2)  $3s^2 3p^3 - 3s 3p^4$  and  $3s^2 3p^3 - 3s^2 3p^2 3d$  fine structure transitions. A correction, due to the M2 component, has been added to the E1 transition probabilities for the two transitions marked with a in Table 3. For all the other cases the E1 component was largely dominant. No radiation of multipole component higher than  $\lambda = 2$  (quadrupole) has been included. In Table 5, we give the transition probabilities from the metastable levels,  $3s^2 3p^2 3d (^3P) ^4F_{9/2}$  and  $(^{1}D) {^{2}G_{9/2}}.$ 

#### 3.2. Electron collisional data

Electron excitation data have been included for fine structure transitions between the 41 levels of the Fe XII model. Collision strengths  $\Omega$  ( $i \rightarrow j$ ) have been computed with the R-matrix technique (Berrington et al. 1987) in the energy range from the excitation threshold to 100 Ry. Details of this scattering computation can be found in BMSI and BMSII; we briefly summarise them here. The calculation was carried out in LS coupling with fine structure interactions in the target incorporated via the term coupling coefficients of Saraph (1972). The target comprised 19 terms, with 121 symmetries ( $LS\pi$  sets) for the

**Table 5.** Spontaneous transition probabilities from the metastable levels in  $3s^2 3p^2 3d$  of Fe XII. Numbers in parenthesis are powers of 10

Transition	A
	$(s^{-1})$
$3s^2 3p^2 3d (^3P) ^4F_{9/2} - 3s^2 3p^3 ^2D_{5/2}^o$	2.759(1)
$3s^2 3p^2 3d (^3P) ^4F_{9/2} - 3s 3p^4 ^4P_{5/2}$	4.451(1)
$3s^2 3p^2 3d (^3P) ^4F_{9/2} - 3s 3p^4 ^2D_{5/2}$	1.422(-1)
$3s^2 3p^2 3d (^3P) ^4F_{9/2} - 3s^2 3p^2 3d (^3P) ^4F_{5/2}$	5.068(-5)
$3s^2 3p^2 3d (^3P) ^4F_{9/2} - 3s^2 3p^2 3d (^3P) ^4F_{7/2}$	8.168(0)
$3s^2 3p^2 3d (^3P) ^4F_{9/2} - 3s^2 3p^2 3d (^3P) ^4F_{9/2}$	5.916(-15)
$3s^2 3p^2 3d (^1D)^2 G_{9/2} - 3s^2 3p^3 ^2 D_{5/2}^o$	2.178(1)
$3s^2 3p^2 3d (^1D)^2 G_{9/2} - 3s 3p^4 {}^4P_{5/2}$	7.614(0)
$3s^2 3p^2 3d (^1D) ^2G_{9/2} - 3s 3p^4 ^2D_{5/2}$	1.494(1)
$3s^2 3p^2 3d (^1D) ^2G_{9/2} - 3s^2 3p^2 3d (^3P) ^4F_{5/2}$	8.834(-2)
$3s^2 3p^2 3d (^1D) ^2G_{9/2} - 3s^2 3p^2 3d (^3P) ^4F_{7/2}$	6.249(1)
$3s^2 3p^2 3d (^1D) ^2G_{9/2} - 3s^2 3p^2 3d (^3P) ^4F_{9/2}$	1.188(2)
$3s^2 3p^2 3d (^1D) ^2G_{9/2} - 3s^2 3p^2 3d (^1D) ^2F_{5/2}$	1.266(-5)
$3s^2 3p^2 3d (^1D) ^2G_{9/2} - 3s^2 3p^2 3d (^3P) ^4D_{7/2}$	4.459(0)
$3s^2 3p^2 3d (^1D) ^2G_{9/2} - 3s^2 3p^2 3d (^3P) ^4D_{5/2}$	3.454(-4)
$3s^2 3p^2 3d (^1D) ^2G_{9/2} - 3s^2 3p^2 3d (^1D) ^2F_{7/2}$	9.599(0)
$3s^2 3p^2 3d (^1D)^2 G_{9/2} - 3s^2 3p^2 3d (^1D)^2 G_{7/2}$	2.783(-1)

 $(N+1)-{\rm e}^-$  complex system ( $l=0\to 16$  for the scattered electron orbital angular momentum quantum number). The radial waves, representing the radial charge distribution of the target, were obtained with a 12 configuration SUPERSTRUCTURE calculation (set 2 of BMSI).

Effective, or thermally averaged collision strengths, are given by

$$\Upsilon(i \to j) = \int_0^\infty \Omega(i \to j) \exp\left(-\frac{E_j}{kT_e}\right) d\left(\frac{E_j}{kT_e}\right)$$
 (1)

where  $E_j$  is the colliding electron kinetic energy after excitation.  $\Upsilon(i \to j)$  values have been provided by BMSI and BMSII for values of electron temperature  $T_{\rm e}$ , spanning the range 4  $10^5\,{\rm K}-10^7\,{\rm K}$ .

# 3.2.1. Electric dipole transitions

The R-matrix collision strengths were topped-up in partial waves using the Coulomb-Bethe approximation and in energy, in order to account for the correct logarithmic trend of  $\Omega(E)$  for this type of transition (Burgess & Tully 1992). This has been thoroughly discussed in BMSII. In the same paper collisional data for these  $3s^2 3p^3 - 3s 3p^4$  and  $3s^2 3p^3 - 3s^2 3p^2 3d$  transitions have been tabulated and discussed.

## 3.2.2. Optically forbidden transitions

For the  $3s^2 3p^3$  fine structure transitions, electron collisional data had originally been calculated with the 102 intermediate state R-matrix computation described in BMSI. For consistency with the E1 scattering data we adopt the new electron excitation rates for these 10 transitions obtained using the 121 intermediate state R-matrix

**Table 6.** Normalised level populations for the lowest 41 fine structure levels in Fe XII.  $T_{\rm e} = 1.5 \ 10^6 \ {\rm K}$ . The numbers in parenthesis are powers of 10. TH88 = Tayal & Henry (1988). F77 = Flower (1977)

Configuration	Level	Λ	$V_{\rm e} = 10^8 \ {\rm cm}^{-3}$		$N_{ m e}$	$=10^{12} \text{ cm}^{-3}$	
		present work	F77	TH88	present work	F77	TH88
$3s^2 3p^3$	${}^{4}S_{3/2}^{o}$	9.71(-1)	9.66(-1)	9.69(-1)	2.70(-1)	1.70(-1)	3.83(-1)
	$^{2}\mathrm{D}_{3/2}^{o}$	2.35(-3)	3.61(-3)	3.79(-3)	1.81(-1)	1.50(-1)	1.51(-1)
	$^{2}D_{5/2}^{o}$	2.66(-2)	3.06(-2)	2.64(-2)	2.78(-1)	2.06(-1)	2.72(-1)
	${}^{2}\mathrm{P}_{1/2}^{o}$	5.41(-5)	7.60(-5)	2.00(-4)	7.16(-2)	7.04(-2)	5.68(-2)
	${}^{2}P_{3/2}^{o}$	6.99(-5)	6.43(-5)	1.64(-4)	1.38(-1)	1.27(-1)	1.37(-1)
$3s 3p^4$	$^{4}P_{5/2}$	8.42(-11)	9.22(-11)	6.28(-11)	2.47(-7)	1.78(-7)	2.85(-7)
	${}^{4}\mathrm{P}_{3/2}$	4.87(-11)	5.65(-11)	3.90(-11)	1.46(-7)	1.08(-7)	1.74(-7)
	$^{4}P_{1/2}$	2.32(-11)	2.75(-11)	1.97(-11)	6.96(-8)	5.25(-8)	8.60 (-8)
	$^{2}D_{3/2}$	2.55(-13)	2.91(-13)	4.91(-13)	8.17(-8)	6.69(-8)	6.84(-8)
	$^{2}D_{5/2}$	1.09(-12)	1.40(-12)	2.04(-12)	1.31(-7)	1.00(-7)	1.27(-7)
	${}^{2}\mathrm{P}_{3/2}$	1.07(-12)	1.19(-12)	9.80(-13)	4.89(-8)	3.09(-8)	4.48(-8)
	${}^{2}\mathrm{P}_{1/2}$	2.42(-13)	3.06(-13)	1.94(-13)	2.21(-8)	1.83(-8)	1.69(-8)
0 0	$^{2}S_{1/2}$	1.50 (-13)	1.77(-13)	3.95(-13)	2.11 (-8)	2.01(-8)	2.62(-8)
$3s^2 3p^2 3d$	$(^{3}P)^{4}F_{3/2}$	2.38(-11)	2.17(-11)		1.48(-7)	9.94(-8)	
	$(^{3}P)^{4}F_{5/2}$	6.38(-11)	5.71(-11)		3.78(-7)	2.49(-7)	
	$(^{3}P)^{4}F_{7/2}$	3.96(-10)	3.55(-10)		2.41(-6)	1.68(-6)	
	$(^{1}D)^{2}F_{5/2}$	4.09(-11)	2.76(-11)		3.74(-7)	2.27(-7)	
	$(^{3}P)  ^{4}F_{9/2}$	1.17(-4)	1.01(-4)		3.45(-2)	1.99(-1)	
	$(^{3}P)^{4}D_{1/2}$	1.15(-12)	1.14(-12)		2.28(-8)	1.58(-8)	
	$(^{3}P)^{4}D_{7/2}$	7.18(-11)	7.66(-11)		1.80(-6)	9.52 (-7)	
	$(^{3}P)^{4}D_{3/2}$	4.92(-12)	4.47(-12)		4.57 (-8)	2.94(-8)	
	$(^{3}P)^{4}D_{5/2}$	7.76(-12)	1.16(-11)		1.08(-7)	6.52(-8)	
	$(^{1}D)^{2}F_{7/2}$ $(^{1}D)^{2}G_{7/2}$	2.31(-7)	2.43(-7)		6.19(-3)	3.47(-3)	
	$(^{1}D)^{2}G_{9/2}$	9.90(-13) $9.62(-7)$	9.47(-13) $7.82(-7)$		1.83(-7) $2.09(-2)$	1.12 (-7) 7.33 (-2)	
	$(^{3}P)^{2}P_{3/2}$	1 1	1 1 .		, ,	1 1.	
	$(^{3}P)^{4}P_{5/2}$	1.24 (-13) $7.15 (-12)$	2.70(-13) $7.80(-12)$		1.48 (-8) 2.04 (-8)	1.08(-8) 1.41(-8)	
	$(^{3}P)^{2}P_{1/2}$	1.02(-13)	1.17(-12)		6.57(-9)	5.57(-9)	
	$(^{3}P)^{4}P_{3/2}$	4.63(-12)	4.57(-12)		1.31(-8)	8.44(-9)	
	$(^{3}P)^{4}P_{1/2}$	2.23(-12)	1.68(-12)		6.45(-9)	4.21(-9)	
	$(^{1}S)^{2}D_{3/2}$	8.03 (-13)	3.05(-12)		1.15(-8)	1.18(-8)	
	${}^{(1)}_{1}^{(1)}^{(2)}^{(3)}_{1}^{(2)}^{(3)}_{1}^{(2)}$	5.07(-13)	5.00(-13)		1.49(-8)	7.61(-9)	
	$(^{1}D)^{2}D_{3/2}$	2.31(-14)	3.20(-14)		9.45(-9)	8.86(-9)	
	$(^{1}D)^{2}D_{5/2}$	1.42(-13)	2.30(-13)		1.60(-8)	1.64(-8)	
	$(^{1}D)^{2}P_{1/2}$	2.41(-15)	2.71(-15)		4.17(-9)	4.54(-9)	
	$(^{3}P)^{2}F_{5/2}$	4.66(-14)	6.74(-14)		1.16 (-8)	1.03(-8)	
	$(^{1}D)^{2}P_{3/2}$	1.01(-14)	2.07(-14)		8.10(-9)	8.13(-9)	
	$(^{1}D) {^{2}S_{1/2}}$	5.70(-15)	8.02(-15)		3.94(-9)	4.49(-9)	
	$(^{3}P)^{2}F_{7/2}$	1.68(-13)	2.12(-13)		1.57(-8)	1.26(-8)	
	$(^{3}P)^{2}D_{5/2}$	2.72(-14)	2.80(-14)		9.69(-9)	9.16(-9)	
	$(^{3}P)^{2}D_{3/2}$	7.11(-15)	9.46(-15)		6.32(-9)	6.36(-9)	

calculation described in BMSII. We note that the inclusion of the extra intermediate states introduced a minor correction to the collisional data, with a largest difference of 2% for the collision strengths and 0.3% for the effective collision strengths.

The remaining optically forbidden transitions include all possible  $3s^2\,3p^3-3s\,3p^4$  and  $3s^2\,3p^3-3s^2\,3p^2\,3d$  transitions and those populating and de-populating the two metastable  $3s^2\,3p^2\,(^3P)\,3d\,^4F_{9/2}$  and  $3s^2\,3p^2\,(^1D)\,3d\,^2G_{9/2}$  levels through excitation and de-excitation within the two excited  $3s\,3p^4,\,3s^2\,3p^2\,3d$  configurations. The inclusion of the complete set of electron excitation data populating and de-populating all the metastable levels of the atomic

system is an essential feature of the level population calculation, as these levels attain considerable population densities with increasing electron density in the plasma (Gabriel & Jordan 1971).

Top-up in partial waves for all these optically forbidden transitions has been performed as described in BMSI. At  $E=100\,\mathrm{Ry}$  the top-up contributions were found to be less than 13% for all transitions. In the BMSI, the collision strength calculation extended to  $E=100\,\mathrm{Ry}$  and no top-up in energy was carried out. For completeness, we have now carried out a top-up in energy using the treatment based on the classification given by Burgess & Tully (1992). According to this, the high energy behaviour

of  $\Omega\left(E\right)$  for optically forbidden transitions should follow a constant or  $E^{-2}$  trend, depending on the role played by electron exchange. We estimate an accuracy for this method of better than 5% for  $\Delta \Upsilon/\Upsilon$  at  $10^7$  K.

Given the fairly large number of  $T_{\rm e}$  points for which effective collision strengths have been computed, it was considered convenient to have  $\Upsilon\left(T_{\rm e}\right)$  values available in a compressed and easily accessible format. The scaling and fitting technique devised by Burgess & Tully (1992) was adopted as a proper approach to our problem. These data will be made available via the CHIANTI database (Dere et al. 1997; Landi et al. 1999); the CHIANTI database is available at the following Internet addresses:

http://www.olar.nrl.navy.mil/chianti.html
http://www.arcetri.astro.it/science/chianti/chianti.html
http://www.damtp.cam.ac.uk/user/astro/chianti/chianti.html

# 4. Comparison of different collisional datasets

The set of statistical equilibrium equations has been solved for our Fe XII model in order to derive the level populations as a function of the electron number density,  $N_{\rm e}$  and electron temperature,  $T_{\rm e}$ . The detailed balance equations may be written as

$$\sum_{j=1}^{n} d_{ij} N_j = 0 i = 1, n (2)$$

where n=41 in our model,  $N_j$  are the unknown level populations, such that  $\sum_{j=1}^n N_j = N$ , N being the total ion density, and  $d_{ij}$  represents the total probability of a j to i transition. This includes the important radiative and collisional processes. The spontaneous radiative decay  $A_{ji}$  is the dominant radiative process. In the present results, photo-excitation and stimulated emission have been neglected. Collisional processes include electron-ion inelastic scattering. The electron collisional rate coefficient  $C_{ij}$  for excitation (i < j) is defined as

$$C_{ij} = \frac{8.63 \ 10^{-6}}{\omega_i T_e^{1/2}} \Upsilon(i \to j) \ e^{\frac{-\Delta E_{ji}}{kT_e}} \tag{3}$$

where  $\Delta E_{ji} = E_j - E_i$  is the transition energy,  $\omega_i$  is the statistical weight of the initial level i and  $\Upsilon(i \to j)$ , the effective collision strength.

It should be noted that proton excitation processes, which should affect fine structure transitions between the closely spaced levels of the ground  $3s^2 3p^3$  configuration, have been shown to be negligible for the Fe XII ion by F77 and Feldman et al. (1983). They have therefore been excluded from the present treatment. Level population densities have been calculated in the electron density range  $10^8-10^{12}$  cm<sup>-3</sup>, in steps of 0.5 in log  $N_{\rm e}$ , and for different temperature values in the region around  $T_{\rm max}$ , the temperature of Fe XII maximum abundance in collisional ionisation equilibrium (1.4  $10^6$  K).

In Table 6 we compare our results with the data provided by Tayal & Henry (1988) at  $T_{\rm e}=1.5~10^6~{\rm K}$  and

for  $N_{\rm e}=10^8$  and  $10^{12}~{\rm cm}^{-3}$ . We also performed a level population calculation using the collision strengths published by F77, coupled to the radiative data discussed in Sect. 3.1. These results are also included in Table 6 for comparison.

From the table it can be seen how the two metastable levels  $3s^2 3p^2 (^3P) 3d ^4F_{9/2}$  and  $3s^2 3p^2 (^1D) 3d ^2G_{9/2}$  attain appreciable populations, comparable with those of the  $3s^2 3p^3$  excited levels at high  $N_{\rm e}$  values. The same is true for the  $3s^2 3p^2 (^1D) 3d ^2F_{7/2}$  level, which is not strictly metastable. However, Table 3 reveals that the only E1 decay channel for this level is down to the  $3s^2 3p^3 ^2D_{5/2}^{\rm o}$  level and that the corresponding transition probability is one of the smallest listed in the table. This explains the anomalously high population and the "pseudo-metastable" behaviour of this level. The populations of these three levels, along with those of the five fine structure levels of the ground  $3s^2 3p^3$  configuration, are several orders of magnitude larger than for the remaining excited levels.

A detailed comparison over the  $10^8-10^{12}$  cm<sup>-3</sup> density range can be made between the different data sets and highlights significant discrepancies. For the five lowest 3s<sup>2</sup> 3p<sup>3</sup> levels we have results available from all three computations. At  $T_e = 1.5 \times 10^6$  K we find, for the ground  ${}^4S_{3/2}^{o}$ level, an average difference of 9% with Tayal & Henry (1988) and of 13% with F77. This discrepancy gets worse with increasing electron density, reaching 42% when comparing with Tayal & Henry (1988) and 37% when comparing with F77. Tayal & Henry (1988) pointed out that, when comparing their results with those obtained using collisional data by F77, the disagreement was considerably greater for the 3s<sup>2</sup> 3p<sup>3</sup> <sup>2</sup>P<sup>o</sup> levels than for the 3s<sup>2</sup> 3p<sup>3</sup> <sup>2</sup>D<sup>o</sup> levels. We find the same result when we compare our results with Tayal & Henry (1988). The normalised level populations for the  ${}^2P^{o}_{1/2}$  and  ${}^2P^{o}_{3/2}$  levels differ by up to about a factor of 3 and 2 respectively. However, when we compare our population data with those obtained using F77 collision strengths, the situation looks quite different, with average differences of 22% and 6% for the  ${}^{2}P_{1/2}^{o}$ ,  ${}^{2}P_{3/2}^{o}$  levels. We find better agreement with F77 than with Tayal & Henry (1988). We believe this is a consequence of the better agreement of our  $3s^2 3p^3 - 3s 3p^4$  collisional data with F77 than with Tayal & Henry (1988), as pointed out in BMSII. For the remaining 3s<sup>2</sup> 3p<sup>2</sup> 3d levels discussed above a comparison is possible only with the results obtained using F77's collisional data. An average difference of 19% is found for the  $(^{1}D)$   $^{2}F_{7/2}$  level population. For the two metastable levels there are much larger differences, particularly at high densities ( $N_e = 10^{12} \text{ cm}^{-3}$ ), more than a factor of 5 for the  $(^{3}P)^{4}F_{9/2}$  level and more than a factor of 3 for the  $(^{1}D)^{2}G_{9/2}$  level.

#### 5. SERTS observations

The SERTS instrument has recorded solar spectra during eight flights over the last eleven years. A description of the instrument is given by Neupert et al. (1992).

Table 7. SERTS-89 Fe XII lines used in the present analysis. Intensities are in erg cm<sup>-2</sup> s<sup>-1</sup> sr<sup>-1</sup>. <sup>a</sup>: see text

λ (Å)	$\lambda_{\mathrm{CHIANTI}}$ (Å)	Intensity (Thomas & Neupert 1994)	Revised intensity (Young et al. 1998)	Comments
186.88	186.88	$1330 \pm 330$	$\frac{(164 \text{mg} \text{ et al. } 1666)}{775 \pm 330}$	blend of Fe XII 186.88 Å and 186.85 Å with
100.00	100.00	1000 ± 000	110 ± 000	S XI 186.88 Å and O III first order 373.81 Å
192.37	192.39	$2370 \pm 340$	300-400	blend with Mn xv first order 384.75 Å
193.51	193.52	$1280 \pm 230$		
195.12	195.12	$1220 \pm 210$		self blend with Fe XII 195.13 Å
$196.62^{a}$	196.65		$280 \pm 140$	line not listed in the original SERTS-89 spectrum
200.41	200.36	$370 \pm 100$	< 100	blend with Ca VI first order 400.83 Å
201.12	201.12	$400 \pm 140$	< 154	blend with Fe XIII 201.12 Å
219.43	219.44	$140 \pm 60$		
$283.70^{a}$	283.45		$18 \pm 9$	line not listed in the original SERTS-89 spectrum
291.01	291.05	$110 \pm 20$		
335.04	335.34	$13 \pm 6$		
338.27	338.28	$77 \pm 10$		
346.86	346.85	$67 \pm 9$		
352.11	352.11	$144 \pm 17$		
364.47	364.47	$233 \pm 26$	$220 \pm 30$	blend with Si Xi 364.5 Å
382.85	382.87	$7\pm2$		

#### 5.1. SERTS-89 observations

The version of SERTS flown in 1989 (SERTS-89) recorded first order solar spectra between 235 and 450 Å, and second order spectra between 170 and 225 Å, with spectral resolutions  $\leq 0.08 \text{ Å}$  and  $\leq 0.04 \text{ Å}$ , respectively. Thomas & Neupert (1994) present an average active region spectrum derived from SERTS-89 spectra. A wealth of strong electric dipole Fe XII lines have been identified in the SERTS-89 spectrum and their ratios subsequently used as plasma diagnostics by Keenan et al. (1996) and Young et al. (1998), henceforth referred to as K96 and Y98, respectively. It should be mentioned that in their diagnostic work, K96 employed theoretical electron excitation data from Tayal & Henry (1988) for the  $3s^2 3p^3 - 3s 3p^4$  transitions and from F77 for the 3s<sup>2</sup> 3p<sup>3</sup>-3s<sup>2</sup> 3p<sup>2</sup> 3d transitions, whereas Y98 used the collisional data from F77 consistently for all transitions. In the present work we used the set of excitation rates discussed in Sect. 3 to compute theoretical line ratios. The Fe XII lines listed in the SERTS-89 catalogue which have been analysed in this work are summarised in Table 7. The wavelengths in the first column are those measured by Thomas & Neupert (1994) from the SERTS-89 spectrum, rounded to two decimal places. For the two lines marked with a, identifications, wavelengths and intensities have been proposed in a later re-analysis of the SERTS-89 spectrum by K96 and confirmed by Y98. For comparison, wavelengths from the energy levels given in the CHIANTI atomic database are given in the second column. These were taken from the NIST database (Martin et al. 1995) and experimental values from Jupén et al. (1993). The intensities in the third column are those reported by Thomas & Neupert (1994), although it should be noted that a subsequent re-evaluation of the absolute calibration scale for SERTS-89 has increased all the original values by a factor of 1.24. This factor can be neglected when working with line ratios, as in the present context. The diagnostic work of Y98 identified blends for some of the lines in Table 7. The revised Fe XII intensities suggested in their paper are given in the fourth column. The identified blends are specified in the last column.

# 5.2. SERTS-95 observations

The version of SERTS flown in 1995 (SERTS-95) incorporated a multilayer-coated diffraction grating that enhanced the instrumental sensitivity in the second order waveband, thus minimising the problem of blends for the important second order lines and bringing out many lines which had not been seen in any of the previous flights. The spectral resolution in second order was  $\sim 0.03$  Å. Brosius et al. (1998b) present average active region and quiet Sun spectra derived from SERTS-95 spatially resolved spectra. The relative radiometric calibration was derived by means of density and temperature insensitive line intensity ratios (Brosius et al. 1998a), an approach originally proposed by Neupert & Kastner (1993). Fe XII lines present in the SERTS-95 active region spectrum are listed in Table 8.

# 6. Theoretical intensity ratios

Line intensity ratios can be divided into three groups for diagnostic purposes.

Branching ratios are formed by transitions which share the same upper level and, therefore, they represent a direct check on the quality of the adopted radiative transition probabilities. Branching ratios are temperature and density insensitive.

The accuracy of the adopted electron excitation rates is, on the other hand, tested by *density insensitive ratios*, whose insensitivity to the plasma electron density

Table 8. Fe XII lines in the SERTS-95 active region and quiet Sun spectra. Intensities are in erg cm<sup>-2</sup> s<sup>-1</sup> sr<sup>-1</sup>

λ (Å)	$\lambda_{\mathrm{CHIANTI}}$ (Å)	$I \pm \sigma_I$	Comments
		Active	region spectrum
186.87	186.88	$500 \pm 60$	self-blend with Fe XII 186.85 Å
192.39	192.39	$210 \pm 25$	
193.51	193.52	$490 \pm 60$	
195.12	195.12	$870 \pm 100$	self-blend with Fe XII 195.13 Å
196.64	196.65	$120 \pm 20$	
198.56	198.56	$52 \pm 10$	blend with S VIII 198.55 Å
211.74	211.73	$94 \pm 30$	
214.40	214.40	$68 \pm 28$	
217.28	217.28	$98 \pm 35$	
219.45	219.44	$74\pm22$	
		Quie	t Sun spectrum
186.89	186.88	$74\pm27$	self-blend with Fe XII 186.85 $\rm \mathring{A}$
192.39	192.39	$99\pm22$	
193.51	193.52	$196 \pm 28$	
195.13	195.12	$312\pm39$	self-blend of Fe XII 195.12 Å and 195.13 Å

originates from the lines being mainly excited from the same lower level, according to

$$N_j A_{ji} = N_e N_i C_{ij}. (4$$

However, a small residual density and temperature sensitivity is sometimes present in these ratios. This is due to non-negligible contributions from levels other than the common lower level to the population of the upper levels of the two transitions. In order to take into account this slight variability, we calculated values of these ratios in the  $N_{\rm e}$  interval  $10^8-10^{12}\,{\rm cm}^{-3}$ , in steps of 0.5 in the log scale, at the temperature of maximum ion abundance  $(\log T_{\rm max} = 6.15)$ . The theoretical ratios used throughout the present work have been obtained as the mean of these values. The calculated standard deviation has been taken as an "error" on the mean due to density effects,  $\delta R_{\rm N}$ . Variations in temperature have been found to be negligible for the ratios involving SERTS-95 lines. In a few SERTS-89 ratios (marked with <sup>T</sup> in Table 9) temperature sensitivity was found to produce greater variability in the ratios than density. In such cases, ratios were calculated at  $N_{\rm e} = 10^{10} {\rm cm}^{-3}$  and for three temperatures, log  $T_{\rm max}$ and log  $T_{\rm max}\,\pm\,0.15$ . The ratios given in Table 9 are those corresponding to  $\log T_{\rm max}$  and the largest scatter in the temperature domain has been taken as an "error"  $\delta R_{\rm T}$ due to temperature effects.

Density sensitive ratios have been computed at the temperature of maximum ion abundance (log  $T_{\rm max} = 6.15$ ). The tabulated error bars have been derived from the observed uncertainties  $\delta R_{\rm obs}$ .

# 6.1. Atomic physics uncertainties

No absolute method of determining the errors on the atomic data exists, but we can examine the covergence of radiative transition data, for example, as the size and quality of atomic basis sets is increased. Comparing the results obtained for oscillator strengths with the scattering target of BMSI (set 2) with their most elaborate calculation (set 3A), we find differences which are typically a few percent. Other possible sources of uncertainty are a) the top-up procedures in l and E for the collision strengths, b) the transformation of the collision strengths from LS to pair coupling and c) the truncation of the target state expansion. These uncertainties are largely unquantifiable. We adopt an uncertainty of  $\delta R_{\rm at}/R$  of 5% for all the ratios with the exception of 219.43/196.62, for which a value of 10% has been estimated.

## 6.2. Theoretical uncertanties

The error bars for the theoretical intensity ratios have been calculated as the rms of the atomic uncertainties  $\delta R_{\rm at}$  and the errors  $\delta R_{\rm N}$  and  $\delta R_{\rm T}$ , depending on which was dominant in the density range of interest. The superscript  $^{\rm N}$  and  $^{\rm T}$  is used to indicate that density or temperature variability is dominant respectively over the atomic uncertainty  $\delta R_{\rm at}$  for the specified ratio.

# 7. Fe XII line ratios in the SERTS-89 spectrum

# 7.1. Density insensitive ratios and branching ratios

In deriving the observed ratios listed in Table 9 we used the original SERTS-89 catalogue intensities tabulated in

Ratio	Theory (present work)	Keenan et al. (1996)	Young et al. (1998)	SERTS-89
382.85/338.27	$0.18 \pm 0.01$		0.17	$0.09 \pm 0.03$
192.37/195.12	$0.30 \pm 0.03^{N}$		$0.25 \pm 0.03$	$1.9 \pm 0.4$
192.37/364.47	$2.7  \pm  0.3^{\mathrm{T}}$	2.55		$11 \pm 2$
193.51/195.12	$0.61 \pm 0.07^{N}$		$0.61 \pm 0.01$	$1.0 \pm 0.3$
193.51/364.47	$5.6  \pm  0.7^{\mathrm{T}}$	6.78		$6 \pm 1$
219.43/196.62	$0.9 \pm 0.1$		$0.73 \pm 0.04$	$0.5 \pm 0.3$
219.43/186.88	$0.20 \pm 0.01$		$0.21 \pm 0.05$	$0.2 \pm 0.1$
291.01/219.43	$0.6 \pm 0.2^{N}$		$0.41 \pm 0.06$	$0.8 \pm 0.4$
364.47/195.12	$0.11 \pm 0.02^{\mathrm{T}}$	0.09	$0.13 \pm 0.01$	$0.18 \pm 0.04$
346.86/364.47	$0.33 \pm 0.02$	0.37	$0.35 \pm 0.01$	$0.31 \pm 0.05$
352.11/364.47	$0.65 \pm 0.03$	0.70	$0.67 \pm 0.01$	$0.7 \pm 0.1$

**Table 9.** Comparison of Fe XII theoretical density insensitive ratios with SERTS-89 observations of a solar active region. The 186.88 Å and 364.47 Å line ratios have been calculated with the revised intensity value by Young et al. (1998)

third column of Table 7 for all the lines, with only two exceptions: the 186.88 Å line and the 364.47 Å line, for which the intensity values proposed by Y98, corrected for the contributions of the identified blending lines, have been used. We note in Table 7 that the two strong lines at 186.88 Å and 195.12 Å are Fe XII self blends with 186.85 Å and 195.13 Å, respectively. The theoretical values of all the density insensitive, as well as sensitive ratios, involving these two lines have been calculated considering both blending transitions. We note that only the 195.12 Å component was considered in the theoretical ratios published by K96 and Y98.

The only branching ratio found in the list, 382.85/338.27, is in good agreement with Y98, thus confirming their conclusion that the 338.27 Å line is blended. Two candidates for this blend are listed by Thomas & Neupert (1994) as Ar VIII 338.18 Å and Si VIII 338.38 Å.

The two ratios involving the 192.37 Å line, 192.37/195.12 and 192.37/364.47, show a severe disagreement with the observations. This was pointed out by Y98 and K96 respectively. It is due to a known blend of the Fe XII 192.37 Å line with the Mn xv first order 384.75 Å line.

The 193.51/364.47 ratio shows good agreement between theory and observations. However, 193.51/195.12 ratio suggests either a blend in the 193.51 Å observed intensity with an unknown weak first order line, or that the second order 195.12 Å line is too weak relative to the 193.51 Å. The 364.47/195.12theoretical ratio is marginally below the lower limit of the observed value and compares reasonably well with Y98, if allowance is made for the missing 195.13 Å blending component in their theoretical value. Thus we confirm that the problems in the 193.51/195.12 ratio are due to the 195.12 Å line. A similar, although less marked, behaviour is found also with the SERTS-95 spectra (see Sect. 8.1). For this reason, we use the 193.51 Å line for density diagnostics. The K96 theoretical results are in worse agreement with observation, almost certainly due to their use of the Tayal & Henry (1988)  $3s^23p^3-3s3p^4$ electron collisional data.

Three ratios involve the 219.43 Å line. The 219.43/186.88 ratio shows reasonable agreement between theory and observation, after the correction to the 186.88 Å observed line intensity. The theoretical 219.43/196.62 ratio is in marginal agreement with the observed value. The results from SERTS-95 show much better agreement of this theoretical ratio with the observations, which suggests that the 196.62 Å feature in the SERT-89 spectrum is blended with a first order line at around 393.2 Å. There is agreement between the calculated and observed 291.01/219.43 ratio. This is mainly due to the marked variability with electron density ( $\pm$  40%) in the  $10^8-10^{12}~{\rm cm}^{-3}~N_{\rm e}$  range. Density sensitive ratios (see next section) show that the 291.01 Å line is blended with an unidentified line.

 $0.5 \pm 0.1$ 

Within the tabulated uncertainties, our 346.86/364.47 and 352.11/364.47 theoretical ratios show excellent agreement with the SERTS-89 values. In particular we note that the K96 theoretical value for the 346.86/364.47 ratio disagrees with the observed value derived by using the revised intensity for the Fe XII 364.47 Å line. The disagreement becomes worse when using the intensity given in the original SERTS-89 calibration scale, which they adopted in their paper.

Finally, for the 283.70/338.27 ratio we list our theoretical result which replicates that of Y98. No SERTS-89 value has been tabulated in Table 9 for this ratio, due to the identification problems for the 283.70 Å SERTS-89 feature, as discussed in Y98.

The two lines at 200.41 Å and 201.12 Å are blended and the revised intensities provided by Y98 are too uncertain to allow a detailed comparison with theory, so these lines are not considered in the present work.

#### 7.2. Density sensitive ratios

In Table 10 we list the electron densities, on a log scale, derived from SERTS-89 observed ratios using the theoretical line ratios. In view of the results of the previous section, in this section we only use those lines whose density insensitive ratios showed no problems with

Table 10. Solar active region densities derived by comparing Fe XII theoretical density sensitive ratios with SERTS-89 observations. "Unreliable" ratios involve lines whose theoretical density insensitive ratios disagree with observations

Ratio	Present work	Present work (revised intensities)	Keenan et al. (1996)	Young et al. (1998)
		Reliable or potentially	reliable lines	
186.88/193.51	$10.55^{+0.30}_{-0.40}$	$9.95^{+0.50}_{-0.90}$		
219.43/193.51 186.88/364.47	$9.85^{+0.40}_{-0.70} \ 10.55^{+0.30}_{-0.35}$	$10.05^{+0.4}_{-0.6}$	$11.0^{+0.3}_{-0.3}$	
219.43/364.47	$9.85^{+0.40}_{-0.65}$	$9.95^{+0.4}_{-0.7}$	$9.6^{+0.6}_{-0.6}$	
283.70/364.47	$9.8_{-0.60}^{+0.35}$ $9.3_{-0.45}^{+0.25}$	$9.85^{+0.3}_{-0.5}$ $9.35^{+0.25}_{-0.40}$	$9.7^{+0.4}_{-0.4}$	
335.04/364.47 382.85/364.47	$9.3_{-0.45}^{+0.45}$ $9.7_{-0.45}^{+0.35}$	$9.35_{-0.40}^{+0.3}$ $9.8_{-0.4}^{+0.3}$	$9.0_{-0.4}^{+0.4}$ $9.3_{-0.4}^{+0.4}$	
		<u>Unreliable li</u>	<u>nes</u>	
219.43/195.12	$10.45^{+0.50}_{-0.70}$			$10.0^{+0.5}_{-0.7}$
186.88/195.12	10.0+0.45	$10.60^{+0.55}_{-0.75}$	10.1+0.6	$10.1^{+0.4}_{-0.6}$
196.62/364.47 200.41/364.47	$10.6^{+0.45}_{-0.85}$ > 12.0	$10.65_{-0.8}^{+0.5}  10.9_{-1.8}^{+0.7}$	$10.1^{+0.6}_{-0.6}$ > 11.2	
201.12/364.47	$\geq 12.0$ $\geq 11.25$	$10.9_{-1.8}^{+0.50}$ $10.95_{-1.15}^{+0.50}$	$\frac{-}{11.2^{+0.4}_{-0.4}}$	
291.01/364.47 338.27/364.47	$\begin{array}{c} -0.5^{+0.25}_{-0.30} \\ 10.5^{+0.15}_{-0.20} \end{array}$	$10.6_{-0.30}^{+0.125}  10.55_{-0.20}^{+0.15}$	$10.3_{-0.2}^{+0.2}  10.1_{-0.2}^{+0.2}$	$10.3^{+0.2}_{-0.2}$

observations ("reliable lines"), or were not available ("potentially reliable lines").

For comparison purposes, we list the intensity ratios for the lines which we consider not reliable for electron density measurements, together with the corresponding results obtained by K96 and Y98. The first set of densities, in the second column, have been derived from ratios calculated with the original SERTS-89 line intensities and have been included for ease of comparison with K96. Revised intensities, after the subtraction of known blends, have been used to derive the electron densities listed in the third column. These densities should therefore be considered as our final results.

the "reliable" intensity Among ratios, 335.04/364.47 ratio yields a much lower density than all the other ratios in this class. Y98 associate the 335.04 A line with Fe XII, despite the fact that the CHIANTI wavelength for this transition is 335.34 Å. Near this wavelength we find the Mg VIII line at 335.23 Å, identified as blended with the very strong Fe XVI 335.41 Å line by Y98. If, as suggested by Y98, the Mg VIII line is lost in the Fe XVI line, this should happen to the Fe XII line also, whose wavelength is even closer to the Fe XVI line than the Mg VIII line. This argument leads us to cast some doubt on the identification of the 335.04 Å line as Fe XII.

The high density obtained with the 186.88/195.12 and 219.43/195.12 ratios confirms the problems with the 195.12 Å line intensity. The 196.62/364.47 and 291.01/364.47 ratios again lead to much higher densities than previously reported. Possible, as yet unidentified blends for the 196.62 Å and 291.01 Å lines would solve this problem while explaining the discrepancies between theory and experiment for the density insensitive

ratios discussed in the previous section. Y98 argue that the maximum predicted values of the 200.41/219.43 and 201.12/219.43 density sensitive ratios (0.58 and 0.93 respectively) lead to considerable blends in the 200.41 Å and 201.12 Å lines of the SERTS-89 catalogue. We confirm their result and report maximum theoretical ratios of 0.41 and 0.70 respectively. The identified blends for these two lines have been listed in Table 7. The densities listed in Table 10, derived from the revised 200.41/364.47 and 201.12/364.47 ratios, point to rather large estimates for the Fe XII components of the blends, as reported in Table 7. As suggested by Y98, other components are likely to account for the observed intensities of those features. The high electron density found from the 338.27/364.47 ratio confirms the blend for the 338.27 Å feature suggested by the branching ratio reported in the previous section.

The remaining seven "reliable" ratios in Table 10 all lead to densities which, within the error bars, agree well with each other. The mean value deduced from those ratios is  $\overline{\log N_e} = 9.9$ . We note that, by averaging the densities obtained from the same ratios by K96, we would obtain a mean density of  $9.4 \pm 0.5$ , lower than our value. Their reported mean density of  $9.7 \pm 0.4$  is due to their inclusion, in the mean, of the three ratios involving the 196.62 Å, 291.01 Å and 338.27 Å lines, which we have discussed in relation to new possible blends. It is interesting to note that, in their work too, those same three ratios lead to densities distinctly higher than the average value. This further confirms our suspicion that indeed previously unidentified blends might affect the 196.62 Å, 291.01 Å and 338.27 Å observed intensities. The average electron density of around  $\overline{\log N_{\rm e}} = 10$  quoted by Y98 is similar to the values obtained with our atomic data.

This agreement is misleading, because the ratios quoted by Y98 also include lines whose density insensitive ratios showed problems.

It is important to note that our average electron density  $\overline{\log N_{\rm e}}=9.9$  is in broad agreement with previous estimates for active regions ( $\log N_{\rm e}\cong 9.7$  in K96 and  $\log N_{\rm e}\cong 9.8$  in Tayal et al. (1989) from Fe XII diagnostics;  $\log N_{\rm e}\cong 9.5$  in Brickhouse et al. (1995) from Fe XIII line ratios).

However, if we consider the electron densities obtained from ions of different elements observed in the SERTS-89 spectrum, whose temperature of formation (given by Thomas & Neupert 1994) is similar to the Fe XII temperature of formation, we find lower values. Y98 report the following electron densities: Si X - log  $N_{\rm e}=9.1\pm0.2;$  Si XI - log  $N_{\rm e}=9.2\pm0.2;$  Fe XII - log  $N_{\rm e}=9.2\pm0.3;$  Fe XIII - log  $N_{\rm e}=9.5\pm0.2.$ 

Recent analyses of SERTS-89 data have been carried out using accurate atomic data produced as part of the IRON Project for Fe IX (Storey & Zeippen 2001) and Fe XIV (Storey et al. 2000). The electron densities derived for the SERTS-89 spectrum were log  $N_{\rm e}=9.3\pm0.5$  and log  $N_{\rm e}=9.5\pm0.3$  respectively.

For the SERTS-89 spectrum, the Fe XII diagnostic ratios seem to provide higher values of the electron density than the other ions. A similar result is also found with SERTS-95 results (see Sect. 8.2). This problem will be addressed in Sect. 9.

# 8. Fe xII line ratios in the SERTS-95 solar spectrum

#### 8.1. Density insensitive ratios

In Table 11 we present results for selected density insensitive ratios, specified in the first column. For comparison, results obtained using the collision strengths by F77 coupled to Fe XII radiative data from BMSI, are listed in the second column (F77). In the last two columns we report the SERTS-95 observed ratios for both the active region (AR) and quiet Sun (QS) spectra. No ratio is given for the 198.56 Å line due to the reported S VIII blend.

The lines of the multiplet at 192.39 Å, 193.51 Å and 195.12 Å show agreement, within the error bars, between theoretical and both sets of observed data. In contrast, the F77 theoretical value for the 192.39/195.12 ratio does not agree with the SERTS-95 quiet Sun observation. The problem found for the 195.12 Å line in Sect. 7 has disappeared. This indicates that this problem was due to the SERTS-89 observed intensity being less accurate than the SERTS-95 one, and not to the atomic data. Good agreement between theory and observation is also found for the 196.64/186.87 ratio, for both sets of theoretical results. This shows that the line blend affecting the 196.64 Å SERTS-89 intensity was due to a first order line at around 393.2 Å, whose contribution is negligible in the SERTS-95 dataset.

For the two ratios involving the 211.74 Å line, the F77 values have a large density variability in the  $N_e$ range  $10^8$ – $10^{12}$  cm<sup>-3</sup>. This is denoted by the superscript N in Table 11. In our theoretical results for the ratios 211.74/186.87 and 211.74/196.64, we also obtain some density variation,  $\pm 33\%$  and  $\pm 25\%$ , respectively. The difference between our results and those of F77, is due to an order of magnitude difference in the electron collision strength for  $3{\rm s}^2\,3{\rm p}^3\,\,^4{\rm S}^{\rm o}_{3/2}$  –  $3{\rm s}^2\,3{\rm p}^2\,3{\rm d}\,\,(^3{\rm P})\,^2{\rm P}_{1/2}$  (see BMSII). For the ratios 211.74/186.87 and 211.74/196.64 we find disagreement and marginal agreement, respectively, between theory and observation. This seems to point to a blending problem for the 211.74 Å line, although no candidate is found in the CHIANTI atomic database or in available solar line lists (Behring et al. 1976; Dere 1978; Malinovsky & Heroux 1973; Thomas & Neupert 1994).

A severe disagreement is found between the SERTS-95 data and both sets of theoretical results for the two ratios 214.40/192.39 and 214.40/193.51. This problem would not be solved even by assuming a larger atomic uncertainty  $\delta R_{\rm at}$  for the 214.40 Å theoretical line (see discussion in Sect. 6). We are forced to conclude that some previously unreported line might be blended with the Fe XII transition at 214.40 Å.

The same disagreement, although less marked, affects the two ratios 217.28/186.87 and 217.28/196.64. In this case a possible blend for the Fe XII 217.28 Å line is reported by Brosius et al. (1998b) as due to Fe XXII (line at 217.29 Å in CHIANTI). This has to be taken with caution as that line, belonging to the very hot Fe XXII ion, does not even appear in the solar flare line list of Dere (1978).

There is agreement between the observed and computed 219.45/186.87 and 219.45/196.64 ratios, within the error bars. A potential blend in the Fe XII 217.28 Å line, discussed above, would explain the discrepancy of the branching ratio 219.45/217.28 observed in the SERTS-95 active region spectrum with theory.

#### 8.2. Density sensitive ratios

Table 12 presents the Log  $N_{\rm e}$  values derived from selected active region (AR) and quiet Sun (QS) SERTS-95 observed Fe XII ratios. Results of our 41 level Fe XII model are compared with F77.

A density diagnostic for the quiet Sun is possible using the four Fe XII lines listed in Table 8. We derive an average electron density of  $9.1^{+0.4}_{-0.3}$ , using the F77 collisional model, and  $9.5^{+0.5}_{-0.4}$  using the our atomic model. We note that the latter value is in excess of that reported by Brosius et al. 1998b from a similar Fe XIII diagnostic  $(8.8^{+0.1}_{-0.2})$ , whereas the former result (F77) is in better agreement.

More serious problems show up when attempting to derive a density diagnostic for the SERTS-95 active region. The available, and reliable, intensity ratios are formed by the lines at 186.87 Å and 196.64 Å relative to the triplet at 192.39 Å, 193.51 Å and 195.12 Å, and they are reported in Table 12. Average electron densities of  $10.0 \pm 0.2$  and

SERTS-95 SERTS-95 Ratio Theory F77 present work AR QS $0.5\,\pm\,0.1$ 192.39/193.51  $0.41 \pm 0.05^{N}$  $0.48 \pm 0.02$  $0.42 \pm 0.07$  $0.30 \pm 0.03^{\rm N}$ 192.39/195.12  $0.22 \pm 0.01$  $0.24 \pm 0.04$  $0.32 \pm 0.08$  $0.54 \pm 0.07^{N}$  $0.61 \pm 0.07^{N}$ 193.51/195.12  $0.56 \pm 0.09$  $0.6\,\pm\,0.1$ 196.64/186.87  $0.28 \pm 0.04$  $0.22 \pm 0.03$  $0.24 \pm 0.05$ 211.74/186.87  $0.72 \pm 0.61^{N}$  $0.09 \pm 0.03^{N}$  $0.19 \pm 0.06$ 211.74/196.64  $2.34 \pm 1.92^{N}$  $0.4 \pm 0.1^{N}$  $0.8 \pm 0.3$  $0.055 \pm 0.009^{N}$ 214.40/192.39  $0.042 \pm 0.004$  $0.3 \pm 0.1$ 214.40/193.51  $0.022 \pm 0.002$  $0.020 \pm 0.002$  $0.14 \pm 0.06$  $0.09 \pm 0.02^{N}$ 217.28/186.87  $0.084 \pm 0.005$  $0.20 \pm 0.08$  $0.32 \pm 0.07^{N}$ 217.28/196.64  $0.37 \pm 0.04$  $0.8 \pm 0.3$  $0.22 \pm 0.06^{N}$ 219.45/186.87  $0.20 \pm 0.01$  $0.15 \pm 0.05$  $0.8 \pm 0.2^{N}$ 219.45/196.64  $0.9 \pm 0.1$  $0.6 \pm 0.2$ 

Table 11. Fe XII density insensitive line ratios. Both components in the self-blending 186.87 Å and 195.12 Å have been considered

Table 12. Solar active region and quiet Sun densities derived from Fe XII density sensitive line ratios

 $2.4\,\pm\,0.1$ 

Ratio	SER	SERTS-95 AR		RTS-95 QS
	F77	present work	F77	present work
186.87/192.39	$10.0^{+0.2}_{-0.2}$	$10.7^{+0.2}_{-0.2}$	$8.8^{+0.5}_{-0.3}$	$9.4^{+0.6}_{-0.3}$
186.87/193.51	$10.1^{+0.2}_{-0.2}$	$10.5^{+0.2}_{-0.2}$	$0.1^{+0.5}$	$9.5^{+0.5}_{-0.3}$
186.87/195.12	$10.1^{+0.2}_{-0.2}$	$10.5^{+0.2}_{-0.2}$	$9.1_{-0.3}^{+0.3}$ $9.3_{-0.4}^{+0.3}$	$9.5^{+0.3}_{-0.5}$
196.64/192.39	$9.9^{+0.2}_{-0.3}$	$10.9^{+0.2}_{-0.2}$		
196.64/193.51	$10.0_{-0.3}^{+0.2}$	$10.7^{+0.2}_{-0.2}$		
196.64/195.12	$10.0^{+0.3}_{-0.3}$	$10.7^{+0.2}_{-0.3}$		

 $2.4\,\pm\,0.1$ 

 $10.7\pm0.2$  are derived when using F77 and our theoretical model, respectively. These values are in serious disagreement with analogous results obtained by Brosius et al. (1998b) from density sensitive line ratios of Fe x, Fe xI, Fe xIII and Fe xIV (log  $N_{\rm e}=9.4\pm0.2$ ).

219.45/217.28

Both the quiet Sun and the active region results obtained with F77 and our atomic data confirm the problems already found with the SERTS-89 spectrum.

# 9. An improved Fe XII atomic model

The analysis of Sects. 7 to 8 has highlighted a potential limitation in the atomic model employed in our diagnostic work, in particular with regard to the derivation of electron density values for the solar plasma. The observational data seem to suggest that some population mechanisms for the  $3\rm{s}^2\,3\rm{p}^3$ ,  $3\rm{s}\,3\rm{p}^4$  and  $3\rm{s}^2\,3\rm{p}^2\,3\rm{d}$  fine structure levels might have been overlooked in our atomic model. In this Section we explore an approximate and extended atomic model which includes a greater number of levels and hence excitation and de-excitation processes.

The proximity of the three odd parity configurations  $3p^5$ ,  $3s\,3p^3\,3d$  and  $3s^2\,3p\,3d^2$  to the even parity  $3s^2\,3p^2\,3d$  configuration implies a large number of possible electric dipole radiative decays connecting levels of opposite parity. Collisonal excitation from the term of the ground configuration  $(3s^2\,3p^3)$  to these odd parity configurations represents a potentially important population mechanism for the  $3s^2\,3p^2\,3d$  excited levels. Similar effects have been

shown to be important for Fe XIV (Storey et al. 2000) and Fe IX (Storey & Zeippen 2001).

Our new Fe XII atomic model has all the fine structure levels belonging to the configurations:  $3s^2 3p^3$ ,  $3s 3p^4$ ,  $3s^2 3p^2 3d$ ,  $3p^5$  and  $3s 3p^3 3d$ , plus the 28 lowest levels of the configuration  $3s^2 3p 3d^2$ . Radiative and electron scattering data for the 41 levels in the configurations  $3s^2 3p^3$ ,  $3s 3p^4$  and  $3s^2 3p^2 3d$  have already been discussed in Sect. 3. Here we extend this model by introducing new atomic data for selected transitions populating the extra levels in the configurations:  $3p^5$ ,  $3s 3p^3 3d$  and  $3s^2 3p 3d^2$ .

#### 9.1. New R-matrix computation

 $0.8 \pm 0.4$ 

The overall structure of the calculation resembles that described in Sect. 3 in relation to the electric dipole  $3s^2 3p^3 - 3s 3p^4$  and  $3s^2 3p^3 - 3s^2 3p^2 3d$  transitions. Contributions from partial waves up to  $l_{\rm max}=19$  have been included in the expansion of the total collision strengths.

All possible  $3s^2 3p^3$ ,  $3s 3p^4$ ,  $3s^2 3p^2 3d$ ,  $3p^5$  and  $3s 3p^3 3d$  thresholds have been included in the Fe<sup>+11</sup> target description. Due to the overlap of the  $3s 3p^3 3d$  and  $3s^2 3p 3d^2$  configurations, the 10 lowest  $3s^2 3p 3d^2$  thresholds were included as well. A total of 5s LS coupling terms have been included in the expansion of the total wavefunction for the target. The additional excited states are tabulated in Table 13. As experimental energies are not yet available for these high lying terms, theoretical energies have been used.

**Table 13.**  $3p^5$ ,  $3s 3p^3 3d$  and  $3s^2 3p 3d^2 LS$  coupling target terms and corresponding theoretical energies included in our 58 term R-matrix calculation

Label	Configuration	Term	$E\left(\mathrm{Ry}\right)$
1	$3s 3p^3 3d$	$^6\mathrm{D^o}$	5.70844
2	$3p^5$	$^2\mathrm{P^o}$	5.84226
3	$3s 3p^3 3d$	$^{4}\mathrm{D^{o}}$	6.22798
4	•	$^4\mathrm{F}^\mathrm{o}$	6.34912
5		$^2\mathrm{S}^\mathrm{o}$	6.62140
6		$^4\mathrm{G}^\mathrm{o}$	6.70680
7		$^{2}\mathrm{G}^{\mathrm{o}}$	6.96755
8		$^4\mathrm{P}^\mathrm{o}$	7.01903
9		$^{4}\mathrm{D^{o}}$	7.06241
10		$^{2}\mathrm{D^{o}}$	7.08002
11		$^4\mathrm{F}^\mathrm{o}$	7.14363
12		$^4\mathrm{P}^\mathrm{o}$	7.23491
13		$^4\mathrm{S}^\mathrm{o}$	7.23862
14		$^2$ F $^{\rm o}$	7.27654
15		$^{2}\mathrm{D^{o}}$	7.44075
16		$^{4}\mathrm{D^{o}}$	7.47159
17		$^{2}\mathrm{P^{o}}$	7.50503
18		$^{2}\mathrm{F}^{\mathrm{o}}$	7.60011
19		$^2\mathrm{G}^\mathrm{o}$	7.66354
20		$^{4}\mathrm{D^{o}}$	7.93048
21		$^{2}\mathrm{D^{o}}$	7.95657
22		$^{2}\mathrm{P^{o}}$	8.04289
23		$^{2}\mathrm{F}^{\mathrm{o}}$	8.04967
24	$3s^2 3p 3d^2$	$^{2}\mathrm{D^{o}}$	8.24326
25		$^4$ G $^{\rm o}$	8.24633
26	_	$^2\mathrm{S}^\mathrm{o}$	8.25235
27	$3s 3p^3 3d$	${}^{2}\mathrm{F}^{\mathrm{o}}$	8.33190
28		$^{2}P^{o}$	8.34251
29	$3s^2 3p 3d^2$	$^{4}\mathrm{D^{o}}$	8.68908
30	$3s 3p^3 3d$	${}^{2}\mathrm{P^{o}}$	8.76402
31	$3s^2 3p 3d^2$	${}^{2}\mathrm{F}^{\mathrm{o}}$	8.79139
32		${}^{4}\mathrm{F}^{\mathrm{o}}$	8.81068
33		${}^{4}P^{o}$	8.83148
34		$^{2}\mathrm{H^{o}}$	8.89662
35	$3s 3p^3 3d$	$^{2}\mathrm{D^{o}}$	8.91585
36	$3s^2 3p 3d^2$	$^{2}G^{o}$	9.02833
37	$3s 3p^3 3d$	$^{2}\mathrm{D^{o}}$	9.14752
38	$3s^2 3p 3d^2$	$^{4}\mathrm{D^{o}}$	9.21736
39	$3s 3p^3 3d$	$^{2}\mathrm{S}^{\mathrm{o}}$	9.22620

These energies, reported in Table 13, have been calculated with SUPERSTRUCTURE using the configuration basis:

 $\begin{array}{l} 3{\rm s}^2\,3{\rm p}^3,\,3{\rm s}\,3{\rm p}^4,\,3{\rm s}^2\,3{\rm p}^2\,3{\rm d},\\ 3{\rm p}^5,\,3{\rm s}\,3{\rm p}^3\,3{\rm d},\,3{\rm p}^4\,3{\rm d},\,3{\rm s}\,3{\rm p}^2\,3{\rm d}^2,\\ 3{\rm p}^3\,3{\rm d}^2,\,3{\rm s}^2\,3{\rm p}\,3{\rm d}^2,\,3{\rm s}^2\,3{\rm d}^3,\,3{\rm s}\,3{\rm p}\,3{\rm d}^3,\\ 3{\rm p}^2\,3{\rm d}^3,\,3{\rm s}^2\,3{\rm p}^24l,\,3{\rm s}\,3{\rm p}^34l,\,3{\rm p}^4)4l \end{array}$ 

where l = s, p, d.

For the expansion of the (N+1)–e<sup>-</sup> collision complex wavefunction we considered all possible combinations of the scattering electron quantum numbers s=1/2 and  $l=0,\ldots,l_{\max}$  with the orbital and spin angular momenta of the LS coupling target terms. Full details of this calculation can be found in Binello (1998).

Collision strengths for all possible transitions between the resulting fine structure levels have been computed at an energy of 9.68 Ry corresponding to the temperature of maximum ion abundance ( $T_{\rm max}=1.5\ 10^6\ {\rm K}$ ). No top-up in partial waves or in energy has been performed on the original R-matrix collision strengths.

#### 9.2. Discussion of results

Radiative decays have been included for all possible electric dipole transitions from the odd parity levels in the  $3p^5$ ,  $3s\,3p^3\,3d$  and  $3s^2\,3p\,3d^2$  configurations to the even parity levels of the  $3s\,3p^4$  and  $3s^2\,3p^2\,3d$  configurations. The radiative data have been calculated with SUPERSTRUCTURE.

Electron excitation data for all possible  $\Delta S \leq 1$  transitions from the five levels of the ground  $3s^2 3p^3$  configuration and from the two metastable  $(^3P) \, ^4F_{9/2}$  and  $(^1D) \, ^2G_{9/2}$  levels of the  $3s^2 \, 3p^2 \, 3d$  configuration up to the levels of the  $3p^5$ ,  $3s \, 3p^3 \, 3d$  and  $3s^2 \, 3p \, 3d^2$  configurations have been included in the extended collisional model.

In order to assess the relative importance of the new collisional transitions introduced in the enlarged atomic model, all the collision strengths  $\Omega\left(E=9.68~\mathrm{Ry}\right)\geq0.1$  for the  $3\mathrm{s}^2\,3\mathrm{p}^3-(3\mathrm{p}^5,\,3\mathrm{s}\,3\mathrm{p}^3\,3\mathrm{d},\,3\mathrm{s}^2\,3\mathrm{p}\,3\mathrm{d}^2)$  optically forbidden transitions have been compared with all those  $\Omega\left(E=9.68~\mathrm{Ry}\right)\geq1$  for the  $(3\mathrm{s}^2\,3\mathrm{p}^2\,3\mathrm{d}\,\,(^3\mathrm{P})^{\,4}\mathrm{F}_{9/2},\,(^1\mathrm{D})^{\,2}\mathrm{G}_{9/2})-(3\mathrm{p}^5,\,3\mathrm{s}\,3\mathrm{p}^3\,3\mathrm{d},\,3\mathrm{s}^2\,3\mathrm{p}\,3\mathrm{d}^2)$  electric dipole transitions. This comparison confirms the importance of electron excitation from the  $3\mathrm{s}^2\,3\mathrm{p}^2\,3\mathrm{d}$  metastable levels in populating the J=9/2 and  $J=7/2~3\mathrm{s}\,3\mathrm{p}^3\,3\mathrm{d}$  and  $3\mathrm{s}^2\,3\mathrm{p}\,3\mathrm{d}^2$  fine structure levels.

# 9.3. Comparison with the SERTS-95 spectra

The same set of SERTS-95 observations of Fe XII lines discussed in Sect. 8 has been reanalysed using theoretical line intensities obtained with the extended atomic model.

The density insensitive ratios listed in Table 14 reveal that a substantial enlargement of the atomic model (from 41 to 143 levels) does not produce a significant change in these line ratios. For this reason the same comments and conclusions given in Sect. 8.1, when comparing the various sets of theoretical results amongst each other and with the SERTS-95 active region (AR) and quiet Sun (QS) observed ratios, apply to the present case.

However, it is in the analysis of the density sensitive ratios, that the most serious problems arise and the use of the extended atomic model seems to make a significant difference, as shown in Table 15. In particular, the average electron density for the quiet Sun derived from the updated theoretical model is found to be  $9.2^{+0.5}_{-0.3}$ , in log scale. This value is in much better agreement with that derived using the collisional data by F77  $(9.1^{+0.4}_{-0.3})$ , and with that for Fe XIII reported by Brosius et al. (1998a)  $(8.8^{+0.1}_{-0.2})$ , than the  $9.5^{+0.5}_{-0.4}$  value obtained with the 41-level model. Similarly, from the SERTS-95 active region

Table 14. Fe XII density insensitive line ratios from SERTS-95, compared with the 41-levels and 143-levels atomic model predictions

Ratio	Theory		SERTS-95	SERTS-95
	41 levels	143 levels	AR	QS
192.39/193.51	$0.48 \pm 0.02$	$0.48 \pm 0.02$	$0.42 \pm 0.07$	$0.5 \pm 0.1$
192.39/195.12	$0.30 \pm 0.03^{N}$	$0.29 \pm 0.03^{\rm N}$	$0.24 \pm 0.04$	$0.32 \pm 0.08$
193.51/195.12	$0.61 \pm 0.07^{\rm N}$	$0.61 \pm 0.06^{N}$	$0.56 \pm 0.09$	$0.6 \pm 0.1$
196.64/186.87	$0.22 \pm 0.03$	$0.23 \pm 0.03$	$0.24 \pm 0.05$	
211.74/186.87	$0.09 \pm 0.03^{N}$	$0.08 \pm 0.02^{\rm N}$	$0.19 \pm 0.06$	
211.74/196.64	$0.4 \pm 0.1^{N}$	$0.4 \pm 0.1^{N}$	$0.8 \pm 0.3$	
214.40/192.39	$0.042 \pm 0.004$	$0.042 \pm 0.004$	$0.3 \pm 0.1$	
214.40/193.51	$0.020 \pm 0.002$	$0.020 \pm 0.002$	$0.14 \pm 0.06$	
217.28/186.87	$0.084 \pm 0.005$	$0.085 \pm 0.005$	$0.20 \pm 0.08$	
217.28/196.64	$0.37 \pm 0.04$	$0.37 \pm 0.04$	$0.8 \pm 0.3$	
219.45/186.87	$0.20 \pm 0.01$	$0.21 \pm 0.01$	$0.15 \pm 0.05$	
219.45/196.64	$0.9 \pm 0.1$	$0.9 \pm 0.1$	$0.6 \pm 0.2$	
219.45/217.28	$2.4 \pm 0.1$	$2.4 \pm 0.1$	$0.8 \pm 0.4$	

Table 15. Solar active region and quiet Sun densities derived from SETS-95 observations, using the 41-levels and 143-levels atomic model predictions

Ratio	SERTS-95 AR		SERTS-95 QS	
	41 levels	143 levels	41 levels	143 levels
186.87/192.39	$10.7^{+0.2}_{-0.2}$	$10.5^{+0.3}_{-0.2}$	$9.4^{+0.6}_{-0.3}$	$9.2^{+0.6}_{-0.3}$
186.87/193.51	$10.5^{+0.2}_{-0.2}$	$10.4^{+0.2}_{-0.2}$	$9.5^{+0.5}_{-0.3}$	$9.3^{+0.5}_{-0.3}$
186.87/195.12	$10.5^{+0.2}_{-0.2}$	$10.3^{+0.2}_{-0.2}$	$9.5^{+0.3}_{-0.5}$	$9.2^{+0.4}_{-0.4}$
196.64/192.39	$10.9^{+0.2}_{-0.2}$	$10.7_{-0.3}^{+0.\overline{2}} \\ 10.5_{-0.2}^{+0.2}$		
196.64/193.51	$10.7^{+0.2}_{-0.2}$	$10.5^{+0.2}_{-0.2}$		
196.64/195.12	$10.7^{+0.2}_{-0.3}$	$10.5^{+0.2}_{-0.3}$		

data we derive a new electron density value of  $10.5 \pm 0.2$ , to be compared with our old value of  $10.7 \pm 0.2$ . The new value is still in disagreement with the average active region density derived from other iron ions  $(9.4 \pm 0.2)$ ; see Sect. 8.2).

# 9.4. Possible improvements to the atomic model

The improved atomic model for Fe XII still has some limitations. However, the comparison with the SERTS-95 observations does go in the right direction: the electron densities derived from Fe XII and other ions are still not consistent, but they are closer.

Further work needs to be done, bearing in mind the following points:

- 1. Collision strengths computed at one energy point only  $(E=9.68\,\mathrm{Ry})$  have been included in the new collisional model, for the extra  $3\mathrm{p}^5$ ,  $3\mathrm{s}\,3\mathrm{p}^3$  3d and  $3\mathrm{s}^2\,3\mathrm{p}\,3\mathrm{d}^2$  levels. The variation of the collision strengths with energy has been neglected;
- 2. No top-up in partial waves has been applied to the R-matrix collision strengths for the new  $3p^5$ ,  $3s 3p^3 3d$ and  $3s^2 3p 3d^2$  levels, therefore neglecting contributions from l > 19;
- 3. The resonance structure in the collision strengths for excitation to the  $3p^5$ ,  $3s\,3p^3\,3d$  and  $3s^2\,3p\,3d^2$  con-

- figurations has been neglected by computing collision strengths in the open channel energy region only;
- 4. The new collisional model was obtained by simply merging the previous set of  $3s^2 3p^3$ ,  $3s 3p^4$  and  $3s^2 3p^2 3d$  effective collision strengths with the newly calculated  $3p^5$ ,  $3s 3p^3 3d$  and  $3s^2 3p 3d^2$  scattering data. By doing so we neglected the effect of new Rydberg series of resonances, converging on  $3p^5$ ,  $3s 3p^3 3d$  and  $3s^2 3p 3d^2$  excitation thresholds and their influence on the previous set of collision strengths. In this context, Storey & Zeippen (2001) have shown that in the case of the Fe IX spectrum, such additional resonances strongly enhance the collisional rates between the metastable levels of the first excited configurations, leading to significant changes in line intensity ratios.

# 10. Summary and conclusions

In this paper we have employed the new set of radiative and electron collisional atomic data for the Fe XII ion, reported in Binello et al. (1998a, 1998b), in the solution of the detailed balance equations for Fe XII. This has provided us with a new set of Fe XII level population densities and, consequently, of line emissivities. Some clear discrepancies with previous Fe XII level populations computed by Tayal & Henry (1988) have been highlighted and explained in terms of using different atomic data in the two

computations. A similar conclusion was reached by comparing our results with those obtained with the atomic data calculated by Flower (1977).

Recent SERTS-89 and SERTS-95 spectral observations of quiet Sun and solar active regions provided a useful means of testing the quality of our results. Several Fe XII spectral lines have been observed by the SERTS instrument and their relative intensities can be used to test the theoretical line ratios. In the present analysis of Fe XII density insensitive ratios we have often found good agreement between theoretical and observed ratios, as well as indications of possible line blends. When the spectral feature was clearly free from blends we found excellent agreement between theory and observation.

Several density sensitive ratios have confirmed the presence of blends in the observed lines. When this is not the case, a comparison with the theoretical ratios provides an estimate of the electron density value for the observed solar regions. The mean SERTS-89 active region density derived from our Fe XII line diagnostics is found to be 9.9, on a log scale. The SERTS-95 active region density was found to be higher (10.7 on a log scale), while the quiet Sun density was found to be 9.5 on a log scale. These values are greater than those obtained with the F77 atomic data.

The density values measured from both the SERTS flights can be compared with measurements derived from ratios of lines of other ions formed at similar temperatures. Our measurements for Fe XII always show greater densities than those from other ions, highlighting a serious discrepancy. Of course, one conclusion might be that the electron density values derived from all the other ions are in error. However, we think this an unlikely scenario, even though the quality of atomic data used for some ions is questionable.

To investigate this discrepancy, the atomic model adopted in the present work has been extended with a new set of configurations, whose excitation and de-excitation coefficients have been calculated for the first time. The new Fe XII model has been tested using the same set of observed line ratios which could not be explained previously. Encouraging, although not conclusive, results have been obtained. In particular, by reanalysing crucial density sensitive ratios formed by reliable, unblended Fe XII lines we found a consistent drop in the derived electron density values. The resulting average decrease in the electron density for both quiet Sun and active region was not sufficient to bring the new values into agreement with analogous results obtained with different ionic species, but represents a step in the right direction.

A critical evaluation of the new atomic model enables some limitations to be identified in the extended set of electron scattering data, and indicates the way forward towards future improvements.

Acknowledgements. This work was financially supported by PPARC. E. Landi acknowledges financial support from a NATO travel grant during his visit to DAMTP in Cambridge, UK.

#### References

Behring, W. A., Cohen, L., Feldman, U., & Doscheck, G. A. 1976, ApJ, 203, 521

Berrington, K. A., Burke, P. G., Butler, K., et al. 1987, J. Phys. B. 20, 6379

Binello, A. M. 1998, Ph.D. Thesis, University of Cambridge Binello, A. M., Mason, H. E., & Storey, P. J. 1998a, A&AS, 127, 545

Binello, A. M., Mason, H. E., & Storey, P. J. 1998b, A&AS, 131, 153

Blaha, M. 1969, A&A, 1, 42

Brickhouse, N. C., Raymond, J. C., & Smith, B. W. 1995, ApJS, 97, 551

Brosius, J. W., Davila, J. M., & Thomas, R. J. 1998a, ApJ, 497, L113

Brosius, J. W., Davila, J. M., & Thomas, R. J. 1998b, ApJS, 119, 255

Burgess, A., & Tully, J. A. 1992, A&A, 254, 436

Corliss, C., & Sugar, J. 1982, J. Phys. Chem. Ref. Data, 11(1), 207

Czyzak, S. J., & Kreuger, T. K. 1967, Proc. Phil. Soc., 90, 623
 Czyzak, S. J., Kreuger, T. K., Martins, P. A. P., Saraph, H. E.,
 & Seaton, M. J. 1970, MNRAS, 14, 361

Davis, J., Kepple, P. C., & Blaha, M. 1976, J. Quant. Spect. Rad. Transf., 16, 1043

Dere, K. P. 1978, ApJ, 221, 1062

Dere, K. P., Landi, E., Mason, H. E., Monsignori Fossi, B. C., & Young, P. R. 1997, A&AS, 125, 149

Eissner, W., Jones, M., & Nussbaumer, H. 1974, Comp. Phys. Commun., 8, 270

Feldman, U., Cohen, L., & Doschek, G. A. 1983, ApJ, 273, 822 Flower, D. R. 1977, A&A, 54, 163

Gabriel, A. H., Jordan, C. 1971, Interpretation of Spectral Intensities from Laboratory and Astrophysical Plasmas, in Case Studies in Atomic Collision Physics, ed. McDaniel & McDowell, North Holland, vol. 2, ch. 4, p. 210

Gabriel, A. H., & Jordan, C. 1975, MNRAS, 173, 397

Harrison, R. A., Fludra, A., Pike, C. D., et al. 1997, Solar Phys., 170, 123

Hummer, D. G., Berrington, K. A., Eissner, W., et al. 1993, A&A, 279, 298

Jupén, C., Isler, R. C., & Träbert, E. 1993, MNRAS, 264, 627 Kastner, S. O., & Mason, H. E. 1978, A&A, 67, 119

Keenan, F. P., Tayal, S. S., & Henry, R. J. W. 1990, Solar Phys., 125, 61

Keenan, F. P., Doyle, J. G., Tayal, S. S., & Henry, R. J. W. 1991, Solar Phys., 135, 353

Keenan, F. P., Thomas, R. J., Neupert, W. M., et al. 1996, MNRAS, 278, 773

Kreuger, T. K., & Czyzak, S. J. 1970, Proc. Roy. Soc. Lond. A, 318, 531

Landi, E., & Landini, M. 1997, A&A, 327, 1230

Landi, E., & Landini, M. 1998, A&A, 340, 265

Landi, E., Landini, M., Dere, K. P., Young, P. R., & Mason, H. E. 1999, A&AS, 135, 339

Malinovsky, M., & Heroux, L. 1973, ApJ, 181, 1009

Mariska, J. T., Feldman, U., & Doschek, G. A. 1980, ApJ, 240, 300

Martin, W. C., Sugar, J., Musgrove, A., et al. 1995, NIST Database for Atomic Spectroscopy, Version 1.0, NIST Standard Reference Database, 61

Mason, H. E. 1994, ADNDT, 57, 305

Mason, H. E., Monsignori, & Fossi, B. C. 1994, A&AR, 6, 123

- Mason, H. E., Young, P. R., Pike, C. D., et al. 1997, Solar Phys., 170, 143
- Neupert, W. M., & Kastner, S. O. 1983, A&A, 128, 181
- Neupert, W. M., Epstein, G. L., Thomas, R. J., & Thompson, W. T. 1992, Solar Phys., 137, 87
- Nussbaumer, H., & Storey, P. J. 1978, A&A, 64, 139
- Petrini, D. 1970, A&A, 9, 392
- Saraph, H. E. 1972, Computer Phys. Commun., 3, 256
- Storey, P. J., Mason, H. E., & Young, P. R. 2000, A&AS, 141, 285
- Storey, P. J., & Zeippen, C. J. 2001, MNRAS, in press

- Tayal, S. S., & Henry, R. J. W. 1986, ApJ, 302, 200
- Tayal, S. S., & Henry, R. J. W. 1988, ApJ, 329, 1023
- Tayal, S. S., & Henry, R. J. W., Pradhan, A. K. 1987, ApJ, 319, 951
- Tayal, S. S., Henry, R. J. W., Keenan, F. P., McCann, S. M., & Widing, K. G. 1989, ApJ, 343, 1004
- Tayal, S. S., Henry, R. J. W., Keenan, F. P., McCann, S. M., & Widing, K. G. 1991, ApJ, 369, 567
- Thomas, R. J., & Neupert, W. M. 1994, ApJS, 91, 461
- Withbroe, G. L., & Raymond, J. C. 1984, ApJ, 285, 347
- Young, P. R., Landi, E., & Thomas, R. J. 1998, A&A, 329, 291